Title

Axonal regeneration is detected after olfactory ensheathing cell or fibroblast transplantation in Sprague-Dawley rats with completely transected spinal cords

Author

Thornton, Michael Andrew

Publication Date

2016

Peer reviewed|Thesis/dissertation

UNIVERSITY OF CALIFORNIA

Los Angeles

Axonal regeneration is detected after olfactory ensheathing cell or fibroblast transplantation in Sprague-Dawley rats with completely transected spinal cords

A thesis submitted in partial satisfaction of the requirements for the degree Master of Science in Physiological Science

by

Michael Andrew Thornton

2016

ABSTRACT OF THE THESIS

Axonal regeneration is detected after olfactory ensheathing cell or fibroblast transplantation in Sprague-Dawley rats with completely transected spinal cords

by

Michael Andrew Thornton

Master of Science in Physiological Science

University of California, Los Angeles, 2016

Professor Patricia Emory Phelps, Chair

Olfactory ensheathing cells (OECs) are unique glia that support axon outgrowth in the olfactory system and have shown some success as a cellular transplant therapy for the recovery of sensorimotor control after spinal cord injury. A pilot study was designed in which 10 female Sprague-Dawley rats received acute transplantation of skin fibroblasts (FB, control, n=5) or OECs (n=5) after a complete mid-thoracic spinal cord transection. All rats were implanted with epidural stimulating electrodes at spinal cord levels L1 and S2 and trained to climb an inclined grid while receiving sub-threshold stimulation for 20 min., 3 times/week for 6 months. We injected the Bartha-152 (EGFP-expressing) strain of pseudorabies virus (PRV) into the soleus and/or tibialis anterior muscles 6 days before termination to identify hindlimb motor circuits and assess connectivity across the injury site. Viral transport to cholinergic somatic motor neurons and premotor interneurons was detected in 8 rats (4 FB, 4 OEC). Three rats (2 FB, 1 OEC) had evidence of viral labeling rostral to the transection site (T3-6), including cholinergic and Chx10-positive V2a interneurons. Serotonergic axons crossed from the rostral to the caudal stump on GFAP-positive astrocyte bridges in 2 of the 3 rats with evidence of PRVeGFP labeling above the

injury site (1 FB, 1 OEC). Together these data imply that long-term axonal regeneration occurred in two of our complete spinal rats after epidural stimulation, climb training, and olfactory ensheathing cell or fibroblast transplantation.

The thesis of Michael Andrew Thornton is approved.

Mark Arthur Frye

Victor R. Edgerton

Patricia Emory Phelps, Committee Chair

University of California, Los Angeles

2016

TABLE OF CONTENTS

LIST OF FIGURES

ACKNOWLEDGEMENTS

This study was supported by the National Institutes of Health under award numbers R01NS54159 and R01NS076976. We thank Dr. Patrick Card for the generous gifts of the PRV viral stocks, and would like to acknowledge NIH funding P40RR018604 in support of the Center for Neuroanatomy of Neurotropic Viruses. We also thank Dr. Larry Schramm for helpful discussions regarding PRV tracing and the autonomic nervous system, Dr. Hui Zhong for the epidural stimulation electrode and cell transplantation surgeries, Dr. Roland Roy for the EMG and spinal cord transection surgeries, Dr. Rana Khankan for the FB and OEC cultures, help with perfusions, and helpful discussions, Khris Griffis for help with climb training and behavioral testing, Anthony Yeung for help with climb training, behavioral testing, and motor evoked potential testing, Aly Mulji for tracing and analyzing lesion sites, Manan Mehta for tracing axons and helping with the 3D reconstruction, and Katie Ingraham and Griselda Yvonne for helpful discussions and lab support.

Introduction and Background

The olfactory system is unique in that olfactory receptor neurons (ORNs) are generated throughout life and continuously project their axons from the periphery to the central nervous system. Olfactory ensheathing cells (OECs) are the specific glial cell type that support ORN axon outgrowth, and OECs are used as cellular transplants to facilitate recovery after spinal cord injury (SCI). Transplantation of olfactory bulb-derived OECs promotes axonal regeneration into the injury site, even in the completely transected rat spinal cord (Takeoka et al. 2011; Ziegler et al. 2011). Additionally, OEC transplantation increases recovery of sensorimotor function after a complete spinal cord transection in rats (Kubasak et al. 2008; Ramón-Cueto et al. 2000; Takeoka et al. 2011; Ziegler et al. 2011) and in humans (Tabakow et al. 2014).

Rehabilitative training significantly enhances the recovery of posture and locomotor function after SCI (Edgerton et al. 2001). Neural circuits intrinsic to the mammalian spinal cord are independently capable of generating bilateral stepping patterns on a treadmill in response to sensory stimulation, and pharmacological interventions can enhance the stepping in the absence of supraspinal input (Edgerton et al. 1992). Rehabilitative training induces activity-dependent plasticity in spinal neural networks that is dependent on the repeated activation of damaged circuits and promotes functional recovery after injury (Edgerton et al. 2004; Lynskey, 2008; Wolpaw and Tennissen, 2001). Furthermore, OEC-transplantation combined with climb training on an inclined grid facilitates long-term axon regeneration and functional recovery in rats with completely transected spinal cords (Ramón-Cueto et al. 2000; Ziegler et al. 2011).

Lumbosacral epidural spinal stimulation (ES) allows for the direct modulation of spinal locomotor networks and can induce locomotion in completely transected rats and cats (Gerasimenko et al. 2003; Iwahara et al. 1992; Lavrov et al. 2006). In addition, ES shows

promise as a therapy for the recovery of standing and stepping after spinal cord injury in humans (Harkema et al. 2011; Rejc et al. 2015). ES activates the networks of the spinal central pattern generators (CPG) that are capable of coordinating oscillatory step-like movements. This effect is facilitated when ES is combined with rehabilitative training and/or the administration of the 5-HT-receptor agonist quipazine in spinal rats (Gerasimenko et al. 2007).

OEC transplantation promotes axon regeneration after SCI.

OEC transplantation into the injured spinal cord promotes axon regeneration and functional recovery in rodents (Kubasak et al. 2008; Ramón-Cueto et al. 2000; Takeoka et al. 2011; Ziegler et al. 2011), but the mechanisms involved are not yet clear. After transection and OEC-transplantation into the spinal stumps, the OECs migrate to the lesion core, make cell-to-cell contact with damaged processes, modulate the inhibitory environment of the injury site, and interact with astrocytes and microglia (Khankan et al. 2016; Lakatos et al. 2003; Li et al. 2005b). Serotonergic (5-HT) axons of the raphespinal tract are involved in locomotion and may exhibit an increased ability to regenerate after SCI (Cornide-Petronio et al. 2011; Ghosh and Pearse, 2014; von Euler et al. 2002). OEC-transplantation reduces acute 5-HT axon dieback immediately after transection (Khankan et al. 2016) and increases long-term 5-HT axon regeneration through the astroglial scar and into the lesion core (Takeoka et al. 2011; Ramon-Cueto et al. 2000). Furthermore, the 5-HT system is an advantageous axon population for studies of regeneration because only a limited number of 5-HT neurons are found in the adult spinal cord (Li et al. 2005a; Lu et al. 2002; Takeoka et al. 2009).

After injury and the subsequent invasion of meningeal fibroblasts, astrocytes become reactive, increase the length of their processes, align in a transverse orientation to seal off the

intact spinal tissue, and secrete chondroitin sulfate proteoglycans that inhibit axon regeneration (McKeon et al. 1999; Fitch and Silver, 2008; Sofroniew, 2009; Wanner et al. 2013). When transplanted into the injured spinal cord, OECs reduce levels of secreted chondroitin sulfate proteoglycans and modulate the morphology of astrocytes near the scar border (O'Toole et al. 2007, Khankan et al. 2016). OEC-astrocyte interactions, therefore, may reduce the inhibitory environment of the injury site and alter the formation of the reactive astroglial scar to facilitate axon regeneration across the injury site (Khankan et al. 2016, Li et al. 2005b). Axonal regeneration is also inhibited by myelin debris, which is abundant in the injured spinal cord (Filbin et al. 2003, Lee and Zheng, 2012). OECs phagocytose myelin debris in the developing olfactory system (Nazareth et al. 2015) and reduce myelin debris following spinal cord transection (Khankan et al. 2016).

OEC-neurite interactions probably involve secreted neurotrophic factors such as nerve growth factor (NGF), brain-derived neurotrophic factor (BDNF) and glial cell-line derived neurotrophic factor (GDNF) (Lipson et al. 2003; Higginson and Barnett, 2011; Runyan and Phelps, 2009; Woodhall et al. 2001). ORNs extend longer processes when co-cultured with OECs compared to hippocampal glia or laminin alone, indicating a role for OECs in axon outgrowth in the olfactory system (Kafitz and Greer, 1999). Furthermore, when co-cultured with hippocampal neurons, OECs increase neurite outgrowth and neuronal survival, and these effects persisted when the neurons were treated with OEC-conditioned media alone (Pellitteri et al. 2009).

In vitro models of CNS injury are useful to study the direct effects of OECs on injured neurons and astrocytes. Following a scratch injury in neuron/astrocyte co-cultures, OECs increased neurite-sprouting into the injured area by providing a physical substrate for neurite

outgrowth and by secreting growth-promoting soluble factors (Chung et al. 2004). In a glial scar-like stretch injury model in which astrocytes and meningeal fibroblasts are co-cultured and subjected to two abrupt pressure pulses, OECs enhance cortical neurite outgrowth particularly when they are directly aligned with the neuronal processes (Khankan et al. 2015). Thus, OECs possess multiple cellular traits that make them an attractive treatment for enhancing repair after SCI.

Regeneration of propriospinal interneuronal circuits after SCI.

The identification of neuronal populations that regenerate after injury is of great importance to understanding spinal cord reorganization and axon regeneration. An attenuated strain of pseudorabies virus (PRV) can be injected into muscles and retrogradely transported into the CNS to transneuronally label the related somatic and autonomic circuits (Card and Enquist, 2014; Enquist, 2002; Rotto-Percelay et al. 1992; Yang et al 1999). Neuronal infection with PRV occurs via nectin-mediated fusion of the viral envelope and plasma membrane at the presynaptic axon terminal (Card and Enquist, 2014). The virion is transported along microtubules to the nucleus, where the viral genome is inserted for viral replication (Card and Enquist, 2014). After newly formed viral capsids are released into the cytoplasm, they undergo secondary envelopment in the Golgi apparatus and are transported in vesicles that are released at synapses to infect secondary neurons (Card et al. 1993). PRV injections into hindlimb muscles result in the primary infection of lumbar somatic motor neurons (SMNs) at the neuromuscular junction and sympathetic postganglionic neurons at the innervation of vascular smooth muscle (Kerman et al. 2003). Reportedly, the blood vessel innervation associated with the hindlimb muscles injected in the present study travel between T10 and L2 (Rotto-Percelay et al. 1992), several segments caudal to our complete mid-thoracic transection model.

PRV injections into hindlimb muscles should label several groups of premotor interneurons that directly regulate SMN output. The developing ventral spinal interneurons were grouped into four main classes (V0, V1, V2, and V3) based on transcription factor expression (Arber, 2012; Goulding, 2009; Pierani et al. 2001; Vallstedt et al. 2001). V0 interneurons express the homeodomain transcription factor Dbx1 and extend their axons across the commissure and into multiple spinal segments (Pierani et al. 2001). A subset of cholinergic V0 interneurons, the V0c or Partition cells, express the transcription factor Pitx2, are located near the central canal, and were recently shown to be the sole source of C-bouton inputs, which directly regulate SMN firing and excitability (Miles et al. 2006, Witts et al. 2014). V1 interneurons express Engrailed-1, and extend their axons ipsilaterally and rostrocaudally for 1-2 segments (Alvarez et al. 2005; Moran-Rivard et al. 2001). These cells differentiate into GABAergic Renshaw cells and proprioceptive 1a inhibitory interneurons and provide direct inhibitory input to SMNs (Alvarez et al. 2005). V2 interneurons are found just dorsal to the developing motor neurons, and express Lhx3 (Thaler et al. 2002). Postmitotically, these cells differentiate into V2a interneurons, which are glutamatergic and express Chx10, and V2b interneurons, which are inhibitory and express Gata2/3 (Dougherty and Kiehn, 2010; Zhong et al. 2010; Zhou et al. 2000). V2 interneurons are unique in that they project their axons caudally across many spinal segments to synapse on SMNs and exhibit multi-segmental control of locomotion (Goulding, 2009). After the injection of a monosynaptic rabies virus into the TA muscle of postnatal day 3 mice (8 d infection), nearly 30% of monosynaptic propriospinal interneurons labeled with rabies-GFP colocalize with Chx10, and they are found as far rostral as C2 (Ni et al. 2014). Lastly, V3 interneurons express Sim1 during development, and comprise an excitatory population of commissural premotor interneuron that regulates rhythmic locomotor activity (Borowska et al. 2013, Zhang et al. 2008).

Reorganization of the spinal circuitry is essential to the recovery of motor function after injury. Many ventral interneurons synapse directly on SMNs, while others form synaptic relays that convey descending locomotor information through multiple synaptic connections (Ni et al. 2014; Arber et al. 2012). After a mid-thoracic dorsal hemisection in rats (Bareyre et al. 2004) or sequential mid-thoracic hemisections in mice (Courtine et al. 2008), propriopsinal interneurons can form new relay circuits that bypass the injured tissue and promote functional recovery of stepping without the long-distance regeneration of supraspinal axons. Additionally, the descending reticulospinal system is capable of regeneration and re-integration with propriospinal circuits after C4 spinal cord hemisection in rats (Filli et al. 2014).

In the current study, we hypothesize that OEC-transplantation, when combined with ES and climb training, will lead to axon regeneration and the recovery of sensorimotor function after a complete spinal cord transection. Furthermore, we propose that the propriospinal circuits promote functional recovery, even after a complete transection, by the formation of relay connections across the lesion site. The advantage of using a polysynaptic neuronal tracer such as PRV is to label the propriospinal circuits that are synaptically connected to SMNs that innervate specific hindlimb muscles. Here, we will 1) use PRV to visualize and identify propriospinal circuits that regenerate after injury, and 2) analyze the architecture, morphology and connectivity of the injury site for evidence of glial scar modification, bridges of astrocytes, and serotonergic axon regeneration.

Materials and Methods

Animals.

All animal experiments were approved by the Chancellor's Animal Research Committee at UCLA and conducted in accordance with the National Institutes of Health guidelines. Rats were housed under standard conditions with free access to food and water. Female GFP-expressing Sprague-Dawley rats (Perry et al. 1999), 8–10 weeks old, were used to obtain skin fibroblasts (FBs) and olfactory bulb-derived olfactory ensheathing cells (OECs) for transplantation. An overdose of ketamine-xylazine was used for euthanasia before the extraction of the olfactory bulbs or abdominal skin biopsies. Female Sprague-Dawley rats (Charles River Laboratories), 10–12 weeks of age, received FB or OEC-transplantation following a complete mid-thoracic (~T8) spinal cord transection and then 6 months of ES and climb training.

Olfactory bulb-derived OEC cultures.

Methods to prepare all OEC primary and immunopurified cultures were similar to those of Ramón-Cueto et al. (2000) and identical to those recently reported (Khankan et al, 2015). OECs were dissected from the first two layers of the olfactory bulb, and meninges and blood vessels were removed. Cells were dissociated in 0.1% trypsin (Invitrogen) and resuspended in a mixture of 1:1 Dulbecco's Modified Eagle's/Ham's F12 medium (D/F medium; Invitrogen) supplemented with 10% fetal bovine serum (FBS; Hyclone) and 1% penicillin streptomycin (P/S; Invitrogen; D/F-FBS). Medium was changed every 2 d. Dissociated OECs were maintained *in vitro* for 5 d and then immunopurified using anti-p75-nerve growth factor receptor antibody (1:5; clone 192; Chandler et al., 1984). Purified OECs were cultured for an additional 7 d and stimulated to divide with D/F-FBS medium supplemented with pituitary extract (20 μg/ml; Invitrogen) and forskolin (2 μM; Sigma-Aldrich).

Fibroblast cell cultures.

Skin biopsies from the abdominal wall were dissociated into fibroblast (FB) cultures as described previously (Khankan et al. 2016, Takashima 2001). The dermis was separated mechanically from the epidermis and hypodermis. Dermal tissue was trypsinized (0.3%) for 10 min at 37°C, and rinsed with D/F-FBS medium. Cells were centrifuged at 365 × g for 5 min before the pellet was resuspended and incubated in 12.5 mg/ml collagenase (Invitrogen) for 1 h at 37°C. The collagenase-cell mixture was filtered, centrifuged, and then resuspended in D/F-FBS supplemented with primocin (0.1 mg/ml; InvivoGen). Primary FBs were plated on culture flasks, maintained at 37°C with 5% CO2, and the medium was changed every 2 d. FBs were passaged one to two times before cell transplantation (12–14 d *in vitro*).

Surgical Procedures.

Implantation of transcranial stimulating electrodes: Ten female Sprague-Dawley rats, 10-12 weeks old, were used for this study. Before the first surgery, rats were deeply anesthetized with 1-2.5% isoflurane gas administered via facemask. A longitudinal incision was made at the midline of the scalp and the skin and fascia were retracted to expose the skull. Two pilot holes were made in the skull with a small screwdriver at 2 mm posterior to lambda and 8 mm anterior to bregma. Two stainless steel screws were inserted into the pilot holes so that the tip of the screws contacted the dura mater. The insulation was removed from the end-portion of a Teflon-coated wire electrode (AS632, Cooner Wire) that was attached to a head-plug connector (Amphenol), and the exposed wire was coiled around each screw (Iyer et al, 2010). The head-plug connector was then secured to the skull with dental cement and small screws.

Implantation of epidural stimulating electrodes: Next, partial laminectomies were performed at spinal levels L2 and S1. The ES electrodes were formed by removing a 1-mm notch of Teflon

coating from two stainless steel wires. The exposed wire surface was placed toward the dorsal surface of the spinal cord and sutured to the dura mater above and below the exposed portion of wire (Ichiyama et al. 2005).

Implantation of hindlimb intramuscular recording electrodes: A second head-plug connector with five Teflon-coated stainless steel wires was attached securely to the skull with small screws and dental cement, as described above. Then, skin and fascial incisions were made to expose the bellies of the tibialis anterior (TA) and soleus muscles bilaterally (Roy et al. 1992). Two wires from the head-plug connector were routed underneath the skin from the cranium to each muscle. A 0.75 mm notch of Teflon insulation was removed from the stainless steel wires and inserted into each muscle using a 23-gauge needle. The electrodes were positioned in the mid-belly of the muscle and secured with two sutures located at the sites where the wire entered the muscle. Proper electrode positioning was verified by observing muscle contractions elicited by stimulation (Gad et al. 2013, Roy et al. 1992). An additional wire with approximately 1 cm of the insulation removed from the distal end was placed subcutaneously in the dorsum of the animal and served as a ground (Gad et al. 2013, Roy et al. 1992). The skin was sutured and disinfected with betadine, and the rats were allowed to recover in an incubator.

Spinal cord injury and cell transplantation.

Three weeks later, a second surgery was carried out after anesthetization with 1-2.5% isoflurane gas administered with a facemask. A skin incision was made at vertebral levels T6 to L1, the paravertebral muscles were retracted, and partial laminectomies were performed at T7 and T8. The dorsal dura mater was incised longitudinally and then laterally at both ends to expose the spinal cord. The spinal cord was completely transected near spinal level T8 with micro-scissors,

leaving the ventral and lateral dura mostly intact. The rostral and caudal stumps were separated and the intact dura mater was scraped with a glass probe.

In the culture room, FBs or OECs were rinsed with HBSS without Ca^{2+}/Mg^{2+} and dissociated with 0.25% trypsin-EDTA. Just before transplantation, cells were rinsed with medium, centrifuged, and resuspended at a concentration of 100,000 cells per microliter in serum-free DMEM. Immediately following the complete spinal transection, FBs (5 rats) or OECs (5 rats) were injected stereotactically into the spinal cord 1 mm rostral and 1 mm caudal to the transection. Four midline injections of approximately 50,000 cells each were performed, starting with the ventral-most injection site (Ramon-Cueto et al. 2000). A stabilization bar was then inserted adjacent to the T7-T13 vertebrae and secured to the spinous processes. After the surgical site was closed and sutured, rats were placed in an incubator until responsive and then returned to individual cages with Carefresh bedding. Animal care, including bladder expressions, was performed three times daily for the first month after spinal cord transection surgery, and twice daily at 12-hour intervals thereafter. Rats were inspected daily for weight loss and dehydration, and were tested weekly for urinalysis using Multistix 10 SG reagent strips (Siemens). Surgeons and investigators were blinded to the cell treatment groups from the time of transplantation until the end of the study.

Epidural Stimulation and Climb Training.

All rats were trained to climb an inclined grid (1-inch x 1-inch holes) at 45, 60 and 90-degree angles from the horizontal plane (Ramon-Cueto et al. 2000; Ziegler et al. 2011). Our inclined grid was connected to a 36-inch tall tower that had a low-friction platform made of Plexiglas on top that was covered with a dark box. Rats were motivated to climb by placing another rat at the top for social motivation, and they also received a food reward when they lifted themselves onto

the slippery platform. The final part of the climbing test is difficult for the rats unless they engage their hindlimbs to push off the grid and onto the platform. All rats also received bipolar lumbosacral epidural stimulation (ES) during their climb training. Individual thresholds for each rat were calculated daily by determining the minimum stimulation voltage necessary to elicit a consistent contraction, detectable to the touch. Rats were then stimulated at 95% of threshold and at a frequency of 40 Hz. ES + climb training sessions were conducted for 20 min., 3x per week, for 6 months, starting 1 month after spinal cord transection. Rats were tested for climbing ability at 2, 4, 6, and 7 months post-injury using the 60 and 90° grid angles.

PRV Tracer Injections.

At 7 months post-transection, all rats received PRV tracer injections into their hindlimb muscles. PRV-Bartha 152 contains the CMV-EGFP reporter gene cassette inserted into the gG locus of the viral genome, and the CMV promoter drives the expression of EGFP in virally infected cells (Card and Enquist, 2014). In this study, GFP that is detected as a result of PRV-Bartha 152 infection will be termed "PRVeGFP" labeling. FB (n=5) and OEC-treated rats (n=5) received PRV Bartha-152 (1.21x10^9 pfu) injections into a total of two hindlimb muscles (soleus and/or TA) at 7 months post-transection. Transcranial motor evoked potentials (MEPs) were recorded in the soleus and TA muscles just before the PRV injections, and the muscles to be injected were chosen based on the presence of MEPs. FB and OEC-treated rats were paired and received PRV injections into the same muscles (Table 1). Additionally, 2 intact control rats received PRV Bartha-152 injections into the TA and soleus muscles unilaterally. Rats were anesthetized with isoflurane and an incision was made to expose the muscle to be injected. The soleus muscle received 4 injections of 2.5 µL of virus (10 µL total), while the TA received 8 injections of 2.5 µL of virus (20 µL total). A glass micropipette attached to a 10 µL Hamilton syringe was used to

target the PRV to the motor end plates, and the micropipette was left *in situ* after each injection for ~2 min to prevent backflow and ensure diffusion of the virus. Intact and experimental rats survived for 6 d before perfusion.

Table 1:

Animal	Transplant Group	Muscles Injected
1	FB	L-TA, R-TA
2	FB	L-Sol, L-TA
3	FB	L-Sol, L-TA
4	FB	L-TA, R-Sol
5	FB	L-Sol, R-Sol
1	OEC	L-TA, R-TA
2	OEC	L-Sol, L-TA
3	OEC	L-Sol, L-TA
4	OEC	L-TA, R-Sol
5	OEC	L-Sol, R-Sol

Tissue Preparation.

Rats were anesthetized with ketamine (90 mg/kg) and xylazine (10 mg/kg) intraperitoneally, perfused intracardially with 4% PLP (Card and Enquist, 2014), and post-fixed in 4% PLP for 2-3 hours. Spinal cords were dissected and placed in a 30% Sucrose solution for 48-72 hours. After sucrose infiltration, the spinal cords were blocked and embedded in OCT (Tissue-Tek), frozen, and stored at -80°C until cryostat sectioning. Sagittal sections (25 µm thick) were slide mounted on a series of 16 slides so that each slide represented 6-7 sections 400 µm apart throughout the spinal cord.

Immunohistochemistry.

To analyze the number and location of the PRVeGFP-labeled neurons above the injury site, four slides containing every 16th section were processed with primary antibodies against GFP

(1:2000, Aves Labs). Slides were rinsed with 0.1M phosphate buffer containing 0.9% NaCl and blocked in normal donkey serum for 1.5 hours. Endogenous biotin, biotin receptors, and avidin binding sites were blocked with an A/B blocking kit (1:1, Vector Laboratories), for one hour before sections were incubated with primary antibody overnight at room temperature. The next day, the sections were incubated with biotinylated secondary antibody (1:750, Jackson Immunoresearch) for 1 hour, and then avidin-biotin-complex (1:200, Vector Laboratories) for 1 hour. The staining was visualized with a brown 3-3' Diaminobenzidine reaction intensified with 0.02% Imidazole.

To evaluate the reporter protein expression in PRV-infected cells, one slide containing every 16th section was processed for immunofluorescence (IF) with primary antibodies against GFP (1:1000, Aves Labs) and acetone-inactivated PRV (Rb133, 1:7500, generous gift from Dr. Pat Card). To identify the PRVeGFP-labeled cells above the injury site (~T3-6), one slide was processed for IF with primary antibodies against GFP (1:1000, Aves Labs) and one additional marker to analyze colocalization with neurons (anti-NeuN, 1:1000, Millipore), GABAergic interneurons (anti-GAD67, 1:3000, EMD Millipore), cholinergic neurons (anti-ChAT, 1:500, EMD Millipore), or V2a interneurons (anti-Chx10, 1:500, Santa Cruz Biotech). Additionally, one slide was processed with primary antibody against 5-HT (1:5000, Immunostar) to identify relationships between serotonergic axons and PRVeGFP-labeled neurons. Slides were rinsed with 0.1M Tris buffer containing 1.4% NaCl and 0.1% BSA (standard IF), or 0.1M Tris buffer containing 1.4% NaCl and .05% Tween-20 (Tyramide Signal Amplification Plus IF, Perkin Elmer), permeabilized, and blocked in species-appropriate serum (donkey serum, Jackson ImmunoResearch; goat serum, Vector Laboratories) for 1.5 hours before primary antibody incubation. Sections were incubated with primary antibody for 24 hours at room temperature

(GFP, PRV, NeuN, 5-HT) or for 72 hours at 4°C (GAD67, ChAT, Chx10). Sections were incubated with species appropriate AlexaFluor 488, 555, 594, or 647 secondary antibodies (1:100–500; Jackson ImmunoResearch), and counterstained with bis-benzimide (1:500, Sigma-Aldrich). Tyramide signal amplification was used to improve sensitivity for GAD67, ChAT, and Chx10 IF.

To analyze the injury site and adjacent rostral and caudal spinal stumps, at least one slide containing every 16th section was processed for IF with primary antibodies against GFP and Glial Fibrillary Acidic Protein (GFAP, 1:1000, BD Biosciences, mouse; 1:10K, Dako, rabbit), and an additional marker to identify serotonergic axons (5-HT), Fibronectin (FN, 1:1000, Dako), or Aquaporin-4 (Aq4, 1:1000, Sigma-Aldrich). Tissue sections were processed as described above with standard IF techniques.

Image Acquisition and Analyses.

Images were obtained using an Olympus AX70 microscope equipped with a charge-coupled device camera (AxioCam HRcRv.2, Carl Zeiss) and image-capture PC software (ZEN 2012, Carl Zeiss). Panoramic photomicrographs were taken of the entire spinal cord section to be analyzed. Confocal images were obtained with a Zeiss LSM 510/800 microscope. All cell count and contour area tracing analyses were conducted with Neurolucida and Neurolucida Explorer (v10, MicroBrightField).

PRVeGFP cell location and size analysis: Twenty-four serial sagittal sections (100 μm interval) from the thoracic segments directly above the injury site (~T3-T6) were analyzed for PRVeGFP-labeling. Recently we reported that in this transplant model, neither FBs nor OECs survive past 8 weeks post-injury (Khankan et al. 2016). Similarly, in the current study no surviving GFP-labeled FBs or OECs were detected near the injury site, and therefore all GFP-labeling was

derived from the PRV Bartha-152-GFP-expressing viral tracer. PRVeGFP-labeled cells were counted if a distinct cell soma and at least one accompanying process were identified. Cell count was normalized to the section area (cm^2) to control for differences in section size. PRVeGFP-labeled cells within Rexed laminae I-V were designated as dorsal, laminae VII, X and IML as intermediate, and laminae VIII and IX as ventral for the cell location analysis. We used a sagittal atlas of the rat thoracic spinal cord (Schramm, LP, Thoracic Sagittal Atlas) to determine anatomical cell locations. Anatomical markers used to identify spinal location in the sagittal sections included the dorsal funiculus and superficial dorsal horn, intermediolateral cell column, the reticulated area of lateral lamina V, central canal, and the ventral funiculus. The long and short axes of each cell body were also measured to calculate cell soma size, and we excluded cells with long axes of less than 10 μm from the analyses.

Neurotransmitter phenotype analysis of PRVeGFP-labeled cells: One slide containing every 16th sagittal section (400 μm interval) just above the injury site was analyzed to determine if PRVeGFP colocalized with markers to identify neurons (NeuN), GABAergic interneurons (GAD67), cholinergic neurons (ChAT), and ventral, glutamatergic V2a interneurons (Chx10). Additionally, PRVeGFP-labeled cell bodies were analyzed for evidence of close apposition of 5-HT axons. If a cell appeared to be colocalized in the fluorescent image, it was reimaged on a Zeiss LSM 510/800 confocal microscope with 25× or 40× objectives for verification.

Injury site analyses: To determine the lesion volume, one slide (every 16th sagittal section, 400 μm interval) was labeled for GFAP and Aquaporin 4 (GFAP-Aq4) to label astrocyte intermediate filaments and processes, and Fibronectin (FN) to label the extracellular matrix in the lesion core. First, we placed a 4000 μm-square grid over the tissue section that was centered at the FN-positive lesion core to standardize the length of each section analyzed (total length = 8000 μm).

To measure the total cord area, GFAP and Aq4-positive spinal tissue was outlined inside the grid. Next, the FN-positive area within the lesion core was traced, and this value was converted to a volume measurement by multiplying by the inter-section interval (i.e., 400 μm) as described in Kubasak et al. (2008). The lesion volume measure was normalized to the total cord volume for each rat. Cysts within the spinal stumps also were measured and the spared tissue area was calculated as follows:

$$(Total\ cord\ area\ -\ Lesion\ core\ area\ -\ Cyst\ area) \div Total\ cord\ area$$

Axon regeneration analyses: As we detected axon regeneration associated with astrocytic protrusions into the injury site, we quantified the number and area of GFAP-positive extensions from the glial scar borders. For these measurements we defined an "astrocyte extension" as a thin projection of GFAP-positive processes that: 1) is no wider than 100 μm, 2) extends rostrocaudally for more than 500 μm, and 3) contains processes that resemble astrocytic morphology. To quantify the extent of 5-HT axon regeneration into the lesion core, we traced the area of immunoreactive axons that extended beyond the GFAP-positive rostral scar border and also counted the number of 5-HT-positive axon bundles that crossed the glial scar border and entered into the lesion core, as described in Khankan et al. (2016). Then, to determine whether or not the presence of astrocyte extensions correlates with 5-HT axon regeneration, we plotted the area of astrocyte extensions against the area of 5-HT axons in the injury site for all 10 FB- or OEC-transplanted rats.

3D Visualization.

To create a 3D rendering of the injury site in the OEC-treated spinal rat with substantial evidence of regeneration, 22 sagittal sections with an inter-section interval of 100 μm were

immunolabeled to identify astrocytes (GFAP), serotonergic axons (5-HT), and PRVeGFP neurons. Panoramic images of the spinal cord sections were compiled into a single image file. Neurolucida was used to make contour traces of GFAP and 5-HT labeling, and to place markers for PRVeGFP-labeled cells. The contours and markers belonging to a single section were grouped using Neurolucida's serial section manager and then assigned to the proper z-value. Sections were overlaid in sequence and aligned to the prior section by matching multiple regions of interest that were consistent across sections (such as the dorsal meninges attached to the meningeal scar). The 3D visualization feature was used to reconstruct the injured spinal cord in 3 dimensions.

Statistical analyses.

Due to our small sample size (n = 5 rats / group), all statistical comparisons for this study were conducted using a resampling 'bootstrap' method (Efron and Tibshirani, 1991). Bootstrap methods use computational simulations of the null hypothesis to make statistical comparisons without relying heavily on underlying assumptions or estimators. Custom scripts were written in R (3.2.2; R Core Team, 2015) to analyze the data. Measurements from each analysis were averaged to obtain a mean for each animal, and the distribution histogram was plotted to evaluate normality. In all cases the data were not normal, and differences in spread and skew indicated the data were from unequal populations. After re-centering the data, the null hypothesis was simulated using the non-parametric bootstrap approximation to generate 95% confidence intervals. Our experimental differences were compared to the bootstrapped 95% confidence intervals, to generate a p-value. To test the correlation between 5-HT axon area and astrocyte extension area in the injury site, we used the R function cor.test and computed Pearson's r. All graphs represent the mean +/- SEM.

Results

PRV-Bartha 152 reliably expresses GFP in infected neurons in the rat spinal cord and medulla. Attenuated strains of PRV that express fluorescent proteins upon replication are powerful tools to trace the neural circuits that regenerate after SCI. We injected PRV-Bartha 152 into the soleus and tibialis anterior (TA) muscles in two uninjured control rats to evaluate the progression of viral infection and extent of retrograde labeling in the intact rat spinal cord. Five to six days after viral injection, we detected ventral neurons that were likely somatic motor neurons (SMNs) in the lumbar enlargement, and they expressed both PRV and GFP (Fig. 1A). In addition, we detected PRV and GFP-labeled neurons in the lumbar intermediate grey matter that are likely premotor interneurons (Fig. 1B). Interestingly, lumbar SMNs often appeared crenated and had markedly lower levels of PRV-expression compared to premotor interneurons (Fig. 1A-B). As SMNs are the first neurons infected in the circuit, they are at a later stage of infection at the 6 day time point compared to second and third-order neurons, and may be entering cellular lysis (Callaway 2008).

We also detected PRV-infected, GFP-labeled interneurons in the mid-thoracic spinal cord and in the cervical enlargement (Fig. 1C). Additionally, some PRV, GFP and 5-HT triple-labeled neurons were found in the nucleus Raphe pallidus of the medulla (Fig. 1D) that likely represent virally-labeled neurons of the serotonergic raphespinal tract that exerts descending control of locomotion. In all regions examined, we observed a close relationship between GFP-expression and immunolabeling with the anti-PRV antibody (Rb133). About 96% of PRV-positive neurons, analyzed from a single slide of the thoracic block (~T3-6), co-expressed the GFP reporter protein. These findings confirm that 1) the Bartha 152 strain of PRV reliably expresses GFP in infected neurons, 2) the level of PRV-expression varies more than GFP-expression depending on

the state of viral infection, 3) 5-HT neurons in brainstem locomotor regions are infected six days after injection into the soleus and TA, and 4) six days post-PRV injection should be the optimal time of infection for our completely transected rats.

PRVeGFP-labeled lumbar SMNs are detected in 8 of 10 rats with complete spinal transections.

To evaluate the extent of axon regeneration after a complete spinal cord injury following FB or OEC-transplantation, and epidural stimulation combined with climb training, we injected PRV-Bartha 152 into the soleus and/or TA muscles that displayed evidence of motor evoked potentials 7 months post-transection. We detected PRVeGFP-labeled, Choline Acetyltransferase (ChAT)-positive SMNs in lamina IX at lumbar levels L3-L6 in 8 out of 10 injected rats (Fig. 2A). The 2 unlabeled rats were excluded from the PRVeGFP-labeled cell characterization analyses. The ChAT-positive ventral roots revealed PRVeGFP-labeled axons that represent the viral entry route into the lumbar enlargement (Fig. 2B). PRVeGFP and ChAT-positive lumbar interneurons were detected both laterally and near the midline, and may include cholinergic Partition cells in laminae VII/X (Fig. 2C, Phelps et al. 1984), which synapse directly on SMNs and are important for locomotion (Stepien et al. 2010; Witts et al. 2014; Zagaraiou et al. 2009). Thus, we confirmed viral transport from the TA and soleus neuromuscular junctions into ChAT-positive lumbar SMNs and cholinergic interneurons.

PRVeGFP-labeled neurons are detected above the injury site in 3 of 8 SMN-labeled, spinal cord transected rats.

Next we asked if the 8 rats with PRVeGFP-labeled, ChAT-positive lumbar SMNs had evidence of retrograde PRV-transport across the complete transection. For these analyses we initially examined the thoracic region just rostral to the transection site (~T3-6). In 2 of 4 FB rats and 1 of

4 OEC-transplanted rats, PRVeGFP-labeled cells were found rostral to the T8 injury site (Fig. 3A-C). To compare the number of PRVeGFP-labeled cells in each transplant group, we used sagittal sections from the ~T3-6 block and analyzed every fourth section for PRVeGFP-expression. The FB-treated rats had normalized averages of 7 and 41 cells/cm^2 whereas the OEC-treated animal averaged 18 cells/cm^2 (Fig. 3D). Cell soma diameter was plotted as a distribution for all cells detected above the injury site regardless of transplant group (Fig. 3G). Mean cell soma diameter was 20.6 μm, and a second peak was observed near 28 μm. Next, we analyzed the location of all PRVeGFP-labeled cells detected above the injury site, first over dorsoventral (Fig. 3E), and then mediolateral (Fig. 3F) gradients. The dorsoventral analysis revealed that 16% of PRVeGFP-labeled cells in both FB and OEC-treated rats were detected in lamina I-V, 75% were located in lamina VII, X, or the IML, and 9% were located in lamina VIII or IX (Fig. 3H). PRVeGFP-labeled cells were spread throughout the mediolateral width of the grey matter, with a slight increase in cell count near the central canal (Fig. 3I, section 6, 7), and a large increase in sections 4 and 9.

Most PRVeGFP-labeled cells detected above the injury site are neurons.

To better characterize the PRVeGFP-labeled cells detected rostral to the transection, we asked how many coexpressed the neuron-specific nuclear antigen, NeuN. We found that ~70% of PRVeGFP-labeled cells coexpressed NeuN (Fig. 4A). Reportedly, NeuN expression can be decreased or absent in damaged or dying neurons (Gusel'nikova and Korzhevsky, 2015), and we found that NeuN expression was reduced in crenated PRVeGFP-labeled cells. Additionally, some small cells (cell soma diameter < 10um) did not express NeuN, and we suggest that these are infected astrocytes or microglia that have phagocytosed the reporter protein. Card et al. (1993) reported that astrocytes can be infected by PRV, but do not possess the cellular machinery

to produce the secondary viral envelope that is essential for exocytosis and viral spread. We confirmed, therefore, that the majority of our labeled cells above the injury site are neurons.

Neurotransmitter phenotype analysis of PRVeGFP-labeled neurons rostral to the transection. To analyze the neurotransmitter phenotype and neuronal identity of the virally labeled cells, we assessed the colocalization of ChAT, GAD67, and Chx10 with PRVeGFP. One slide (6-7 sagittal sections) from each of the three rats with PRVeGFP labeling above the complete transection was processed for each marker.

Some PRVeGFP-labeled neurons above the injury site are cholinergic: Spinal cholinergic interneurons directly regulate the excitability of SMNs during locomotion via C-bouton terminals (Miles et al, 2006), and cholinergic V0 interneurons (V0c) are involved in left-right coordination during locomotion (Zagoraiou et al, 2009). We detected a small number of PRVeGFP-labeled interneurons in the ~T3-6 segment that were ChAT-positive (Fig. 5A1 – B2). About 15% of PRVeGFP-labeled cells colocalized with ChAT (6/40 cells), however 4 of these 6 cells were in or near the IML (Fig. 5C, blue stars), and likely represent sympathetic preganglionic neurons retrogradely labeled from the vascular smooth muscle. Based on their size and location in spinal laminae VII, we suspect that only 2 out of the 6 ChAT-positive, PRVeGFP-labeled cells may be cholinergic propriospinal interneurons (Fig. 5C, green stars).

Only one PRVeGFP-labeled neuron was GABAergic: Renshaw cells, 1a inhibitory interneurons, and V2b interneurons are GABAergic and directly contact SMNs (Dougherty, 2010; Zhou et al. 2000). Therefore, we analyzed GAD67 expression in the thoracic region above the injury site to further characterize the PRVeGFP-labeled neuronal population. Only one of the 31 PRVeGFP-labeled neurons that were analyzed expressed GAD67 (Fig. 5C).

Chx10 is expressed by adult propriospinal interneurons after SCI: Chx10 is a homeodomain transcription factor that marks developing V2a interneurons that provide substantial glutamatergic innervation to SMNs (Ni et al. 2014; Thaler et al. 1999). Figure 6A shows the distribution of Chx10 expression in the embryonic day 16.5 mouse lumbar spinal cord together with Lmx1B, a transcription factor that characterizes excitatory dorsal horn neurons. Initially, we examined Chx10 expression in nuclei of adult spinal interneurons labeled with PRVeGFP in the lumbar spinal cord (Fig. 6B). Most Chx10-positive interneurons were located near or in lamina VII, in the ventral intermediate region (Fig. 6B). Ni et al. (2014) reported that a large population of ventral interneurons that are monosynaptic to SMNs colocalize with Chx10 in young postnatal mice. The colocalization of lumbar PRVeGFP-labeled cells with Chx10 (Fig. 6B-C) confirms the relationship between Chx10-positive V2a interneurons and the soleus and TA locomotor circuits in the adult rat.

Next we analyzed the sections rostral to the injury site (~T3-6) for evidence of Chx10 expression in infected neurons. Nearly 30% of PRVeGFP-labeled neurons expressed Chx10 (12/43 cells, Fig. 6C-D). Thus, thoracic V2a interneurons were retrogradely labeled with PRV above the complete transection. These virally labeled neurons may represent a propriospinal interneuron population that regenerated and formed synaptic circuits with lumbar SMNs after a complete spinal transection.

Many PRVeGFP-labeled neurons above the injury site are contacted by 5-HT axons.

Next, we asked if any of the PRVeGFP-labeled neurons above the injury site were contacted by descending serotonergic axons. The raphespinal 5-HT system directly modulates SMNs and locomotor interneuron circuits (Ghosh and Pearse, 2014), as well as sympathetic preganglionic neurons (Lewis and Coote, 1990; Pickering et al. 1994). To quantify the extent of serotonergic

innervation, we counted PRVeGFP-labeled cells with evidence of directly apposed 5-HT axons (Fig. 4B). About 44% of our PRVeGFP-labeled cells had at least one closely apposed serotonergic axon varicosity (17/39 cells). Thus, a significant proportion of the virally labeled neurons above the injury site appear to be modulated by the descending 5-HT pathway.

Lesion volume is larger in FB than OEC-transplanted rats.

Next, we analyzed sagittal sections from the injury site (~T7-9) to compare the lesion size between the two cell transplant groups at 7 months post-transection. We labeled astrocytes with GFAP and Aquaporin-4 (Aq4) and the fibrotic lesion core with Fibronectin (FN). Seven of the ten rats had a well-defined FN-labeled separation in the lesion core (Fig. 7A), whereas the remaining three rats (2 OEC, 1 FB) had one or more bridges of astrocytes located dorsomedially across the injury site (Fig. 7B). The total cord area, FN-positive lesion core, and the cysts within the spinal stumps were outlined and measured as shown in Figure 7C. The lesion core area measurements were converted to volumes by multiplying by the inter-section interval (i.e. 400 μm). The lesion volume ratio (lesion volume normalized to total cord volume) was larger in the FB compared to the OEC-treated rats (Fig. 7D, FB, 0.14; OEC, 0.09, p=.046). Cyst volume and spared tissue volume did not differ between cell transplant groups.

An OEC-transplanted rat showed substantial axon regeneration across the injury site.

We observed extensive regeneration of 5-HT-labeled axons across the injury site in one of our OEC-transplanted rats (Fig. 8A). The 5-HT axon bundles extended across the transection site along several GFAP-labeled astrocyte bridges, and coursed into the caudal stump (Fig. 8B-C, white arrowheads). Furthermore, PRVeGFP-labeled neurons in the caudal stump were detected within 100 μm of the descending 5-HT axons (Fig. 8C, yellow arrowhead). In about half of the

analyzed sections a complete lesion through the ventral white matter was observed (Fig. 8D), whereas the other half had extensive dorsomedially-located astrocytic bridges between the rostral and caudal scar borders (Fig. 8A, sections 1-3).

Due to the evidence of axon regeneration, we processed 22 sagittal sections of the injury site (~T7-9) spaced evenly throughout the spinal cord width (100 μm interval) to create a 3D reconstruction. We traced the GFAP-positive area to produce an image of the tissue architecture (Fig. 8 E-G), 5-HT labeling to visualize descending axon bundles (Fig. 8E-G), and identified all PRVeGFP-labeled neurons (Fig. 8E). The GFAP labeling narrowed into thin astrocyte bridges in the injury site that appeared translucent in the 3D reconstruction (Fig. 8 E-F, yellow arrowheads) and allowed us to approximate the damage at the injury site (Fig. 8E, dotted line). There were 714 PRVeGFP-labeled cells in the area caudal to the complete transection, 44 cells within the estimated injury site, and 65 cells in the rostral stump. This pattern of PRV-labeling in the OEC-treated rat strongly suggests that the virus was transsynaptically transported across the injury site (Fig. 8E, green dots). Bilateral descending tracts of 5-HT-immunoreactive axons are seen in the rostral stump, but the axon bundles appear more disorganized at the injury site (Fig. 8E-G, yellow). An enlargement of the injury site revealed descending 5-HT axon bundles extending into the caudal stump tissue (Fig. 8G, white arrowheads) in addition to the apparent regeneration of PRVeGFP synaptic connections.

Compared to FBs, OEC-transplanted rats have more 5-HT bundles crossing the rostral glial scar border.

To quantify the extent of 5-HT axon regeneration, we counted the number of points at which 5-HT axon bundles crossed the rostral GFAP-positive border and entered into the lesion core (Fig. 9A). The mean number of axon bundles crossing the rostral scar border was significantly greater

in OEC than FB-treated rats, even after it was normalized to the measurement of the GFAP-border trace (Fig. 9C, n=5 rats per group, p =.04). As a second measure, we traced the area of 5-HT-positive axons extending into the lesion core (Fig. 9B). The mean 5-HT area in FB-transplanted rats was 55203 um^2 compared to 84720 um^2 in OEC-transplanted rats (Fig. 9D, n= 5 rats per group, p=.14*)*.

Astrocyte bridges are detected in both FB and OEC-transplanted rats.

To determine the extent that astrocytes bridged the injury site we quantified the number and area of GFAP-positive extensions that protruded from the rostral and caudal stumps (Fig. 9B). FB-transplanted rats had an average of 1.4 astrocyte extensions per animal whereas OEC-transplanted rats averaged 2.1 (p=.23). In both FB and OEC-treated rats, there was a trend that the number of GFAP-labeled extensions was greater on the rostral than the caudal side (Fig. 9E, p=.08*,* p=.19) and that there were more GFAP extensions from the caudal stump in OEC than FB-treated rats (Fig. 9E, p =.10). The area of astrocyte extensions in the injury site did not vary by transplant type (Fig. 9F). With only 5 rats per transplant group, differences were frequently not significant, however these data combined may show a trend that OEC-transplantation increases astrocyte bridging into the injury site.

We then examined the relationship between 5-HT axons and astrocyte bridges in the injury site. Figure 10A illustrates an example of an astrocyte bridge in a FB-treated rat that contains bundles of 5-HT axons. Additionally, a retrogradely-labeled, PRVeGFP-labeled axon (white arrow) crosses the injury site in the same section. A high magnification confocal image of the axon bridge revealed a group of astrocytes that extended their processes rostrocaudally and associated with 5-HT axons (Fig. 10B). To quantify the relationship between GFAP-positive astrocyte bridges and regenerating 5-HT-positive axons, we plotted the area of the astrocyte

bridges against the area of the 5-HT axons in the injury site for all 10 spinal rats. A strong correlation was observed between these measures (Fig. 10C, r =.83, p =.003). Furthermore, two of the three rats that had PRVeGFP labeling above the complete transection also had large areas of astrocyte bridging and 5-HT axons in the injury site (Fig. 10C, red boxes). Interestingly, the third rat with PRVeGFP-labeling above the injury site did not have any evidence of 5-HT axon or astrocytic regeneration in the injury site (Fig. 10D). The observed relationships suggest that descending 5-HT axons regenerate into the lesion core on astrocyte-rich bridges after FB or OEC transplantation and epidural stimulation combined with climb training.

Discussion

After a complete spinal cord transection, FB or OEC transplantation, and 6 months of epidural stimulation combined with climb training, we detected PRVeGFP-labeled neurons in the thoracic segments above the T8 transection in three rats (2 FB, 1 OEC), which suggests that the virus was transported across the injury site through regenerated synaptic circuits. A small percentage of these PRVeGFP-labeled thoracic interneurons were cholinergic, and a substantial percentage expressed the transcription factor Chx10, which marks V2a premotor interneurons. To corroborate the viral tracing data, we examined the injury site for evidence of axon regeneration and astrocyte continuity. We found bridges of astrocytes associated with 5-HT and PRVeGFP-labeled axons that crossed the injury site in 2 (1 FB, 1 OEC) of the 3 rats with PRVeGFP-labeled cells rostral to the injury site. Additional analyses showed that OEC-treated rats had smaller lesion sites and more 5-HT axon bundles that crossed the rostral glial scar border than FB-treated rats. The analysis of the injury site, combined with the viral tracing data, is strong evidence for the regeneration of synaptic connections across the complete transection in these two rats. In addition, the 3D reconstruction of 5-HT axons crossing the lesion core in the OEC-treated rat showed an unprecedented level of axon regeneration after a complete transection.

PRV transport through autonomic vs. locomotor circuits.

Injections of PRV into the belly of hindlimb muscles reliably infect SMNs at the neuromuscular junction and label their cell bodies in the lumbar spinal cord (Jovanovic et a. 2010; Kerman et al. 2003; Rotto-Percelay et al. 1992; Tillakaratne et al. 2010). Additionally, intramuscular PRV-injections retrogradely infect the sympathetic postganglionic neurons that innervate the muscle vasculature and then label the sympathetic preganglionic neurons (SPN) that have their cell bodies in the intermediolateral grey matter (Kerman et al. 2003; Rotto-Percelay et al. 1992). In

addition, there may be some overlap between the brainstem and spinal circuits that provide descending control of SPNs and SMNs (Kerman et al. 2003). Therefore, PRV tracing studies from skeletal muscles must take precautions to isolate or identify the somatic and autonomic labeling. In some cases, a sympathectomy is used to remove the sympathetic innervation of the target muscle and isolate the skeletal muscle-related neuronal circuits (Arriaga et al. 2015; Kerman et al. 2003). In the current study, it was not feasible to perform bilateral sympathectomies in combination with the multiple surgeries and severe complete spinal cord transection. Therefore, PRVeGFP-labeling of the sympathetic system may confound our viral tracing results. We addressed these limitations by 1) using a T8 complete transection model, 2) corroborating the PRV tracing data with analyses of axon regeneration across the injury site, and 3) showing that ~30% of PRVeGFP-labeled interneurons located above the complete transection site express a transcription factor that marks locomotor-related interneurons.

PRV injections into the rat medial gastrocnemius muscle result in the labeling of SPNs located in the spinal segments T10-L2 (Rotto-Percelay et al. 1992). We therefore anticipated that all PRVeGFP-labeling associated with SPNs would be found caudal to the T8 transection. There are, however, factors that lead to substantial variation in the sympathetic connections. SPN axons often ascend or descend across several spinal segments within the sympathetic chain (Wallis and North, 1978; Lichtman et al.1980), a single SPN projects to multiple postganglionic neurons (Lichtman et al.1980; Wallis and North, 1978), and each postganglionic neuron receives axonal projections from SPNs in several different spinal segments (Nja and Purves, 1977).

In our cohort of eight rats with successful PRV infection of SMNs, three showed viral transport above the complete T8 transection, and all three had large PRVeGFP-labeled neurons located near the intermediolateral cell column. Importantly, one FB-transplanted rat that had

PRVeGFP-labeling above the complete transection had no evidence of axon regeneration across the injury site (Fig. 10D), whereas in the other two rats, there was clear evidence of axon connectivity across the injury site (Fig. 8, Fig. 10A, D). We suggest that the PRVeGFP-labeling above the injury site in these two rats represents both autonomic and somatic circuits that regenerated across the complete transection, whereas the labeling detected in the FB-treated rat without evidence of axons crossing the injury site is solely due to viral labeling through autonomic circuits.

Chx10-positive spinal V2a interneurons show increased excitability during locomotion (Husch et al. 2015), exhibit rhythmic firing and membrane potential fluctuations during drug-evoked locomotor-like activity (Dougherty et al. 2010), and are necessary for left-right coordination at varying speeds of locomotion (Crone et al. 2008, Crone et al. 2009). Chx10-positive interneurons that colocalized with PRVeGFP were detected rostral to the injury site in both spinal rats with evidence of axon regeneration across the injury site. No virally labeled Chx10 interneurons were found in the FB-treated rat without axon regeneration across the injury site. Based on the extensive studies that link Chx10 with locomotor function, we suggest that the PRVeGFP-labeled Chx10-positive interneurons above the complete transection represent evidence of multisynaptic circuits associated with the soleus and TA muscles.

Axon regeneration across a complete spinal cord transection.

In this study, we used the most severe SCI model, the complete transection, which resulted in a complete loss of sensorimotor function below the T8 segment. Although partial and contusion injuries better replicate the majority of human SCI cases, a complete transection provides the ability to study axon regeneration and functional recovery without the confounding presence of spared axons (Lukovic et al. 2014).

Propriospinal regeneration: Recent studies used a dorsal hemisection (Bareyre et al. 2004), sequential mid-thoracic hemisections (Courtine et al. 2008; Cowley et al. 2008), or a dorsal over-hemisection (Vavrek et al. 2006) to show that propriospinal interneuronal circuits can regenerate and convey supraspinal locomotor commands to lumbar SMNs. These studies suggested that the propriospinal circuits form new connections with descending supraspinal fibers, and then bypass the injury site to convey this information to lumbar SMNs through multiple synaptic connections (Bareyre et al. 2014; Courtine et al. 2008; Filli et al. 2014; Filli and Schwab, 2015). Our detection of PRVeGFP-labeled, Chx10-positive V2a interneurons in the T3-T6 region suggests that these long-descending propriospinal interneurons regenerated across the injury site and formed connections with soleus and/or TA locomotor circuits. To our knowledge this is the first anatomical demonstration of descending propriospinal axon regeneration across a complete spinal cord injury.

Supraspinal regeneration: We also detected extensive 5-HT axon regeneration associated with astrocyte bridges across the complete transection site. A limited number of 5-HT neurons are found in the adult spinal cord (Takeoka et al. 2009), and therefore the majority of serotonergic axons that are found near the complete mid-thoracic transection are derived from the Raphe nuclei that exert descending control of locomotion (Ghosh and Pearse, 2014) and autonomic function (McCall 1983; Watts et al. 2012). Recently, we reported that OEC-transplantation into the completely transected spinal cord preserves severed 5-HT axons in the lesion core and prevents acute axon dieback (Khankan et al. 2016). Additionally, Takeoka et al. (2011) showed that OEC transplantation facilitated long-term 5-HT axonal regeneration into the lesion core 7-months post transection. Now, we show extensive evidence of 5-HT axon regeneration across the

complete lesion in one FB- and one OEC-treated rat that received 6 months of epidural stimulation combined with climb training. These data suggest that 5-HT axons derived from supraspinal locomotor centers are capable of regeneration across a complete spinal cord transection, and that their growth was likely stimulated by epidural stimulation combined with a voluntary activity, i.e. climbing.

The effects of OEC transplantation on the glial scar.

We detected compelling evidence of regeneration of axonal circuits in two spinal rats, one transplanted with FBs and the other OECs. The OEC rat, however, had a more extensive network of astrocyte bridges that supported larger bundles of 5-HT axons compared to the FB rat (Fig. 8). The "pathway hypothesis," posited by Dr. Geoffrey Raisman, proposed that the regenerative capabilities of OECs, when transplanted after SCI, are largely due to OEC-astrocyte interactions that modify the glial scar border to open 'channels' through which axons can course into the inhibitory lesion core (Li et al. 2005; Li and Raisman, 2007). Additionally, the formation of a reactive astroglial scar may actually promote, rather than impede, axon regeneration across the injury site (Anderson et al. 2016). Khankan et al. (2016) found that astrocyte processes within the spinal scar borders were thinned and elongated when in contact with OECs that survived up to 8 weeks post-transection in immunosuppressed rats. To address the question of whether astrocyte bridges provide a substrate for 5-HT axon regeneration, we plotted the area of astrocyte bridges against the area of 5-HT immunoreactivity within the injury site for all 10 spinal rats. The strong positive correlation (Fig. 10C) shows the close relationship between astrocytes extensions from the glial scar border and 5-HT axon regeneration. Based on previous studies and our current results, we propose that transplanted OECs can exert a lasting effect on the glial scar

border that leads to the formation of astrocyte bridges and facilitates long-term axon regeneration across a complete spinal cord transection.

Figure Legends

Figure 1.

PRV-Bartha 152 injected into the TA and soleus muscles reliably expresses GFP in infected neurons in the uninjured rat spinal cord and medulla. **A-B**, One large, ventral neuron (**A**) and several interneurons located in the intermediate spinal cord (**B**) coexpress GFP (green) and PRV (cyan) in the lumbar enlargement 6 days post-injection. The low level of PRV expression in the large neuron (**A**, white arrowhead) suggests it is at a later stage of infection than the interneurons (**B**). **C**, A cervical interneuron located in lamina X coexpresses GFP and PRV 6 days after infection. **D**, PRV, GFP, and 5-HT-positive neurons (white arrowheads) were found in a coronal section in the nucleus raphe pallidus in the medulla. Three cells are PRV/GFP-positive, but do not express 5-HT (yellow arrowheads). These and the following sagittal spinal cord figures are oriented with rostral to the left and dorsal to the top. Medulla transverse section shown in **D**. CC = central canal. Scale bars **A-B, C, D** = 50 μm.

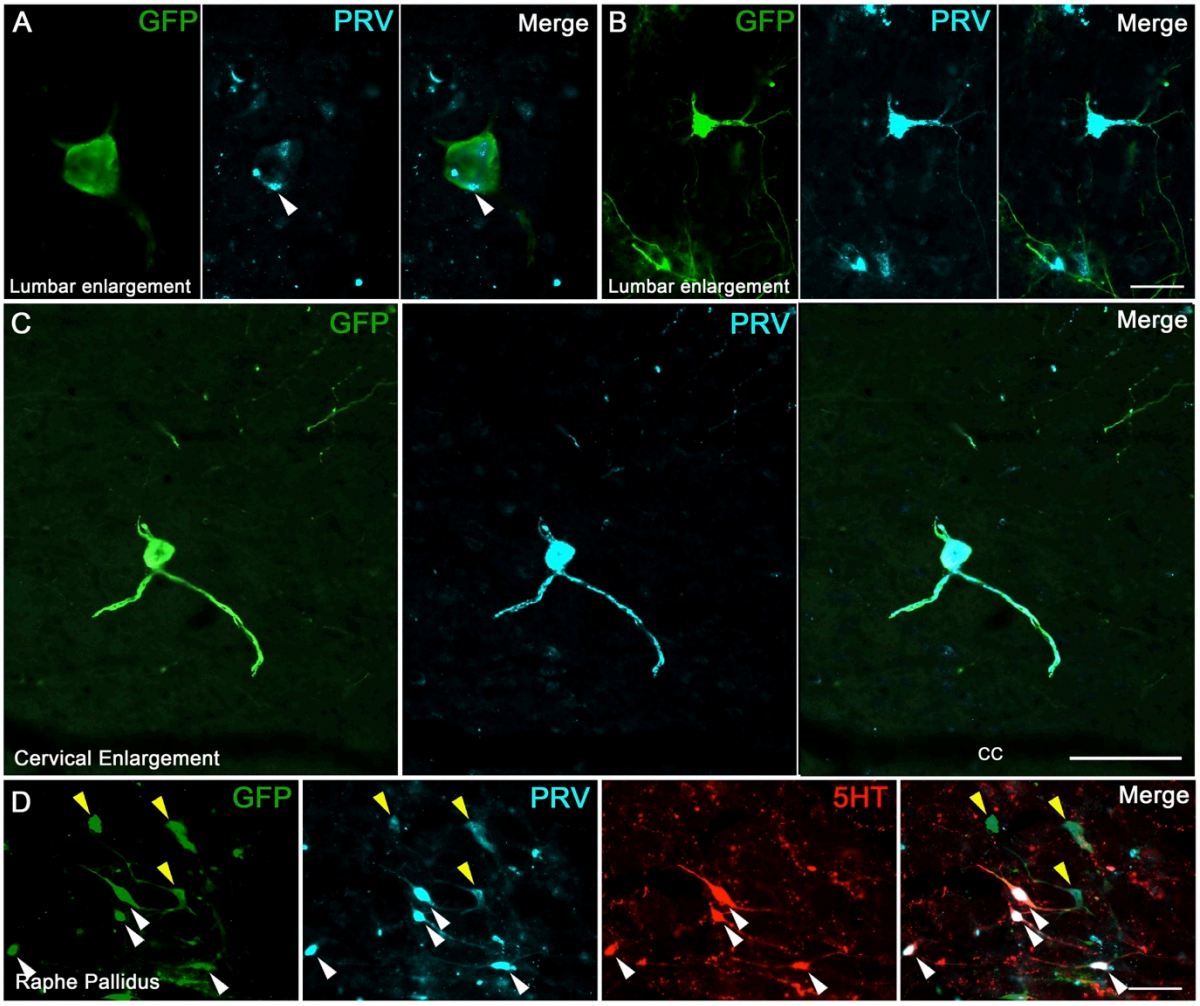
A
GFP
PRV
Merge
Lumbar enlargement
B
GFP
PRV
Merge
Lumbar enlargement
C
GFP
PRV
Merge
Cervical Enlargement
cc
D
GFP
PRV
5HT
Merge
Raphe Pallidus

Figure 2.

ChAT immunolabeling confirms PRV infection of lumbar somatic motor neurons (SMNs) and locomotor-related interneurons. **A**, Five ventral neurons coexpress GFP and ChAT (white arrowheads), confirming the primary viral infection of lumbar SMNs. One large PRVeGFP-positive neuron located more dorsally does not express ChAT (yellow arrowhead), and several ChAT-positive SMNs are not PRVeGFP-labeled (yellow arrows). **B**, A PRVeGFP and ChAT-labeled axon bundle (white arrowheads) is detected in the ventral root at lumbar level L4-L5. **C**, A PRVeGFP and ChAT-labeled interneuron in lamina X may represent a Partition or a Central canal cluster cell. Confocal images represent collapsed z-stack projections of ~20 μm thickness. Scale bars **A, B, C** = 50 μm.

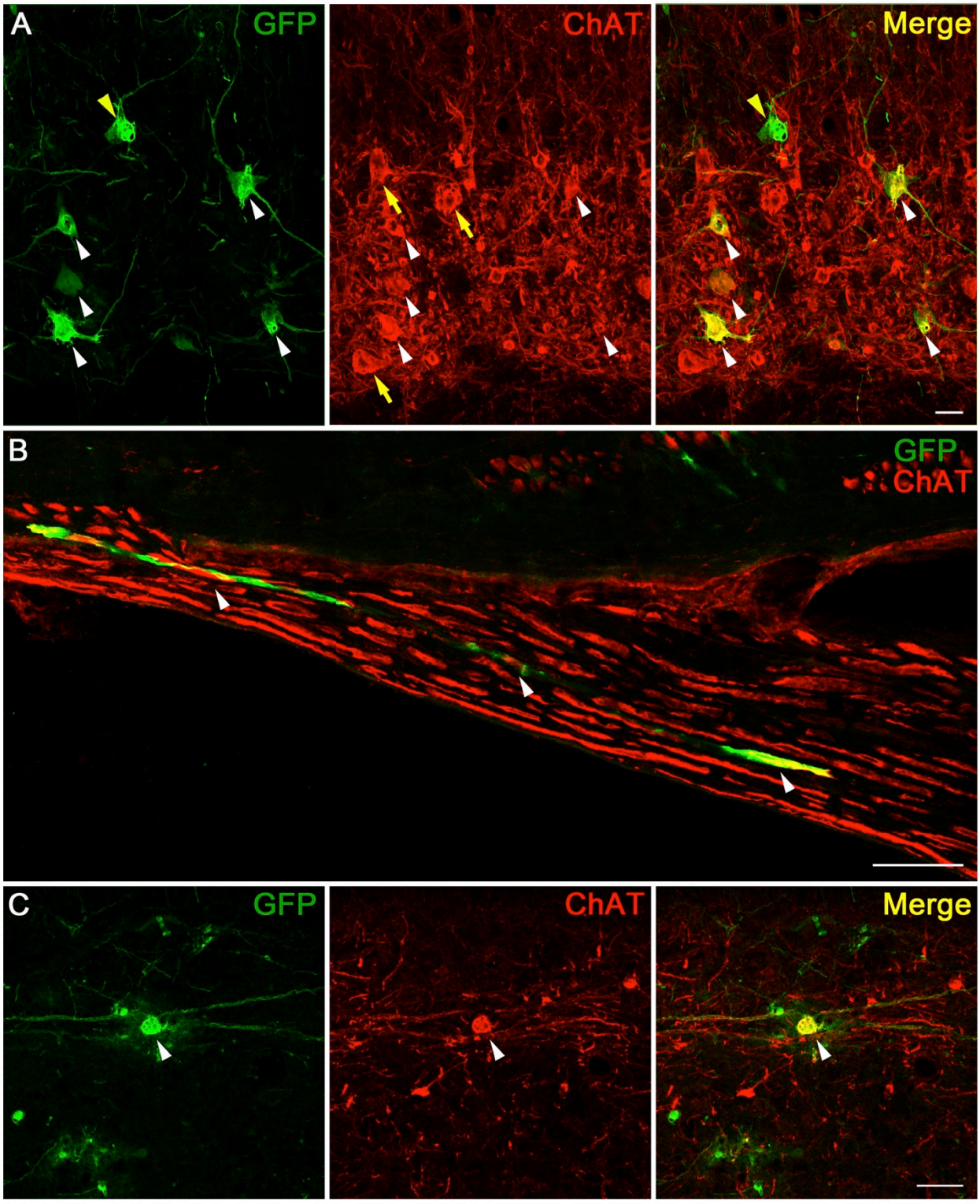
A
GFP
ChAT
Merge
B
GFP
ChAT
C
GFP
ChAT
Merge

Figure 3.

PRVeGFP-labeled cells were detected rostral to the complete T8 transection site in 3 of 8 rats with PRV-infected lumbar SMNs. Two PRVeGFP-labeled neurons (**A**) that were detected in the thoracic intermediate grey matter in an OEC-treated rat. The neuron on the right (white arrowhead) was lysed by the PRV infection, and the diffuse labeling surrounding the cell body is likely the site of reactive astrogliosis. A cluster of PRVeGFP-labeled neurons (**B**, arrowheads) was detected near the intermediolateral cell column (IML) in a FB-treated rat. The ruptured cell somata (**B**, yellow arrowhead) and spherical reaction product surrounding the nuclei indicate post-infection lysis. Two PRVeGFP-labeled neurons (**C**, arrowheads) were found in the thoracic intermediate grey matter of the second FB-transplanted rat, including one with extensive dendritic processes. **D**, PRVeGFP labeling above the injury site was detected in 3 rats (2 FB, 1 OEC). The cell counts were normalized to the area of the tissue of each section, and the mean cell count for each animal is shown in cells/cm^2. PRVeGFP-labeled cells detected in FB and OEC-treated rats were analyzed together to characterize their location. **E-F**, The distribution of PRVeGFP-labeled cells was analyzed within the dorsoventral (**E**) and mediolateral (**F**) gradients of the spinal cord. For the mediolateral location analysis, histograms are binned by 200 μm, with the central canal marked as 0 μm. **G**, Cell soma diameter was calculated as an average of the long and short axes of the somata and plotted as a histogram (n = 91 cells). **H**, Dorsoventral distribution of PRVeGFP-labeled cells detected in all three rats. **I**, Mediolateral distribution of PRVeGFP-labeled cells detected in all three rats. Scale bars **A-C** = 50 μm.

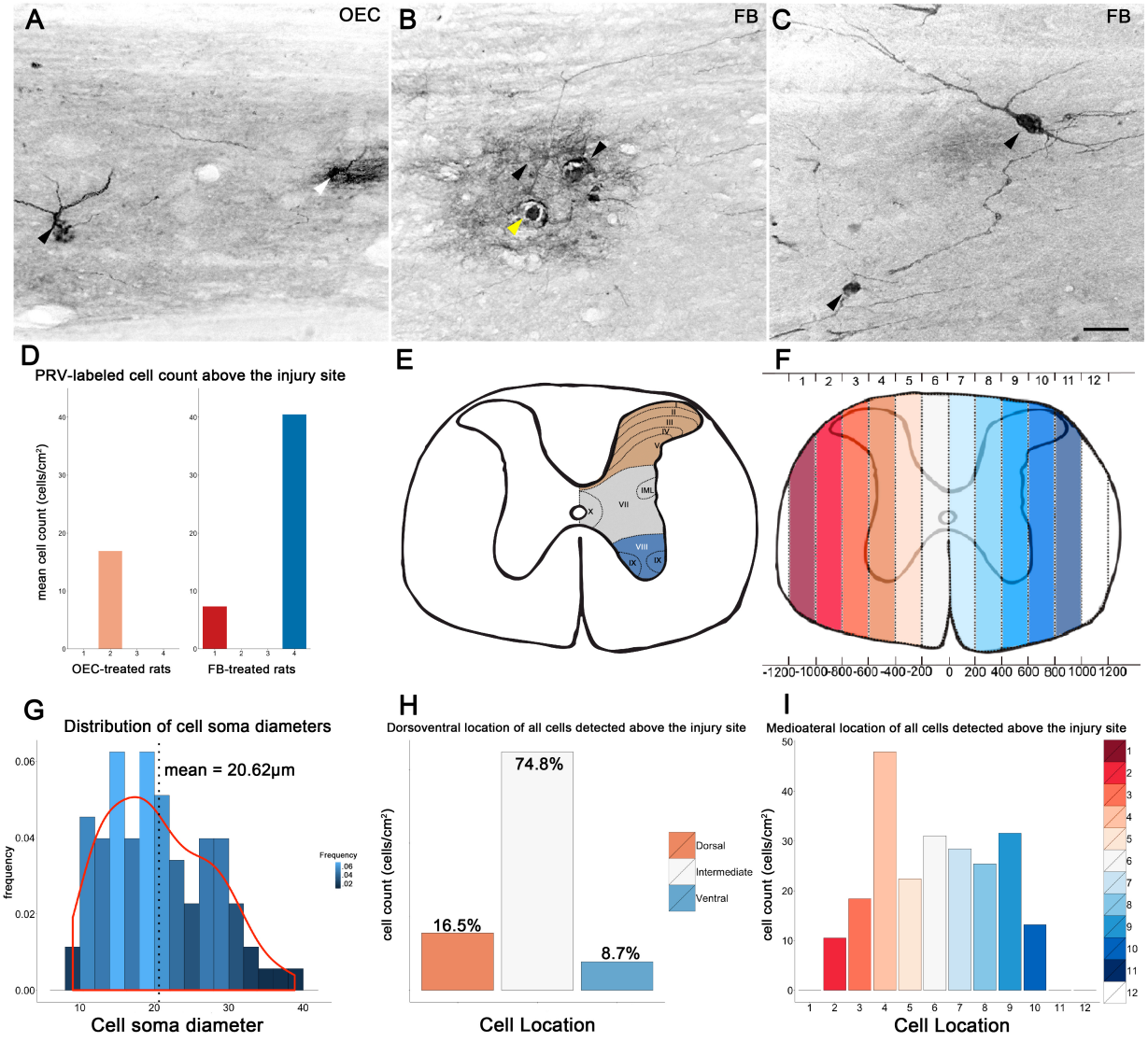
A
OEC
B
FB
C
FB
D
PRV-labeled cell count above the injury site
mean cell count (cells/cm²)
OEC-treated rats
FB-treated rats
E
F
-1200 -1000 -800 -600 -400 -200 0 200 400 600 800 1000 1200
G
Distribution of cell soma diameters
mean = 20.62µm
frequency
Cell soma diameter
H
Dorsoventral location of all cells detected above the injury site
74.8%
16.5%
8.7%
Dorsal
Intermediate
Ventral
cell count (cells/cm²)
Cell Location
I
Medioateral location of all cells detected above the injury site
cell count (cells/cm²)
Cell Location

Figure 4.

PRVeGFP-labeled cells above the transection site (~T3-6) colocalize with NeuN (**A**) and are contacted by 5-HT-positive axons (**B**). **A**, Four PRVeGFP-labeled neurons express NeuN (cyan) in the intermediate thoracic spinal cord (white arrowheads). **B**, A PRVeGFP-labeled neuron in medial lamina VII is contacted by a 5-HT-positive axon (white arrowhead). Confocal image in **A** represents a collapsed z-stack projection of ~20 μm thickness, and in **B** the orthogonal view of a 1.8 μm image slice. Scale bars **A, B** = 50 μm.

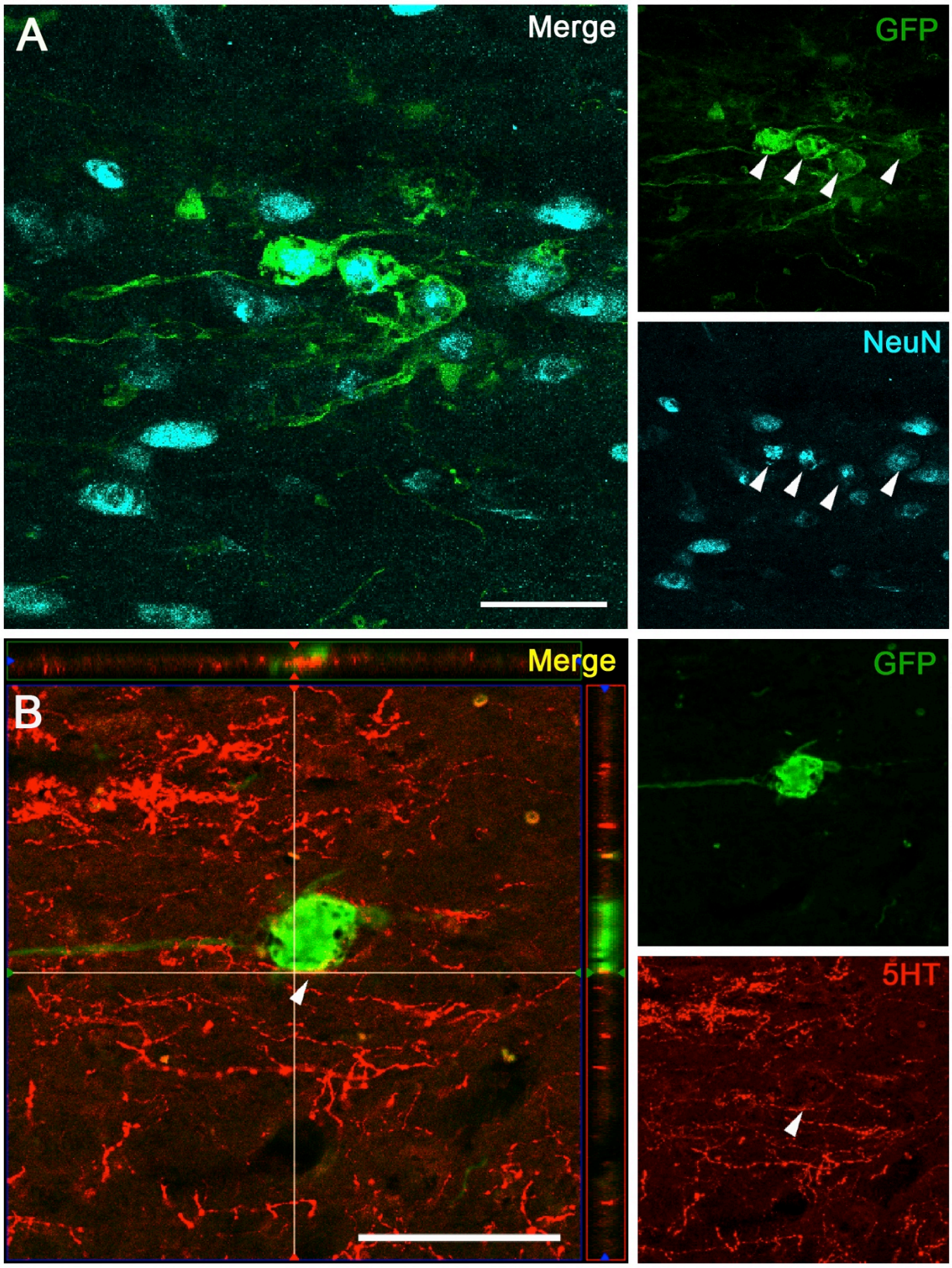
A
Merge
GFP
NeuN
B
Merge
GFP
5HT

Figure 5.

ChAT and GAD67 expression in PRVeGFP-labeled neurons detected above the transection site. **A1**, A PRVeGFP-labeled interneuron dorsal to the central canal colocalizes (white arrowhead) with the PRV antibody (cyan) and expresses ChAT (red). **A2**, Colocalization of PRVeGFP and ChAT-labeling is confirmed in the orthogonal view of the confocal image. **B1**, A cluster of PRVeGFP-labeled cells is located in a lateral section near the IML. One large, PRVeGFP-labeled neuron expresses ChAT (white arrowhead). **B2**, Colocalization of PRVeGFP and ChAT is confirmed in the confocal image. This triple-labeled neuron is most likely a sympathetic preganglionic neuron labeled from the muscle vasculature. **C**, Approximate locations of PRVeGFP-labeled cells from all three animals are mapped on a coronal section. Black dots mark PRVeGFP-only cells, blue stars indicate PRVeGFP and ChAT-labeled cells near the IML, and green stars show PRVeGFP and ChAT-labeled cells in medial lamina VII. Of the 40 PRVeGFP-labeled cells shown, 6 colocalized with ChAT (15%), with four near the IML (10%) and two in laminae VII (5%). **D**, GAD67 expression (red) was detected in one PRVeGFP-labeled cell body out of 31 analyzed. Orthogonal view of the confocal slice suggests colocalization as opposed to GAD67-positive terminal contacts on the PRVeGFP-labeled cell. Confocal images in **A2**, **B2**, **D**, are orthogonal views from 1.8 μm images; Scale bars: **A1**, **B1**, **D** = 50 μm.

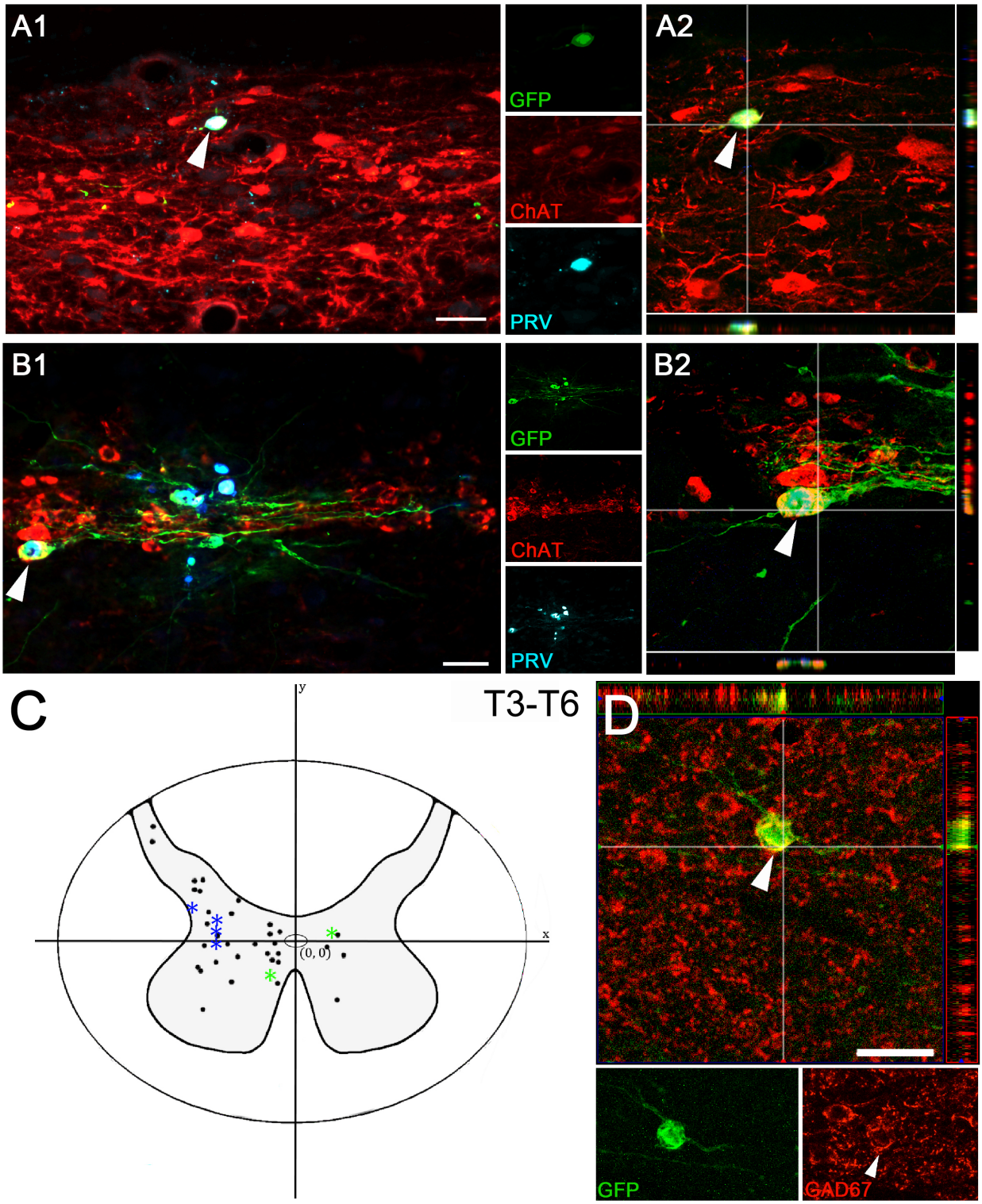
A1
GFP
ChAT
PRV
A2
B1
GFP
ChAT
PRV
B2
C
T3-T6
y
x
(0, 0)
D
GFP
GAD67

Figure 6.

PRVeGFP-infected interneurons express Chx10 in the rat spinal cord. **A**, Chx10 expression (red) is shown in a coronal section of an embryonic day 16.5 mouse spinal cord. Chx10 marks V2a interneurons that are found in the ventral and intermediate spinal cord. Lmx1b is a transcription factor that labels dorsal excitatory neurons and is shown in green to identify the dorsal horn. **B**, Sagittal section of adult rat lumbar enlargement illustrates many Chx10-labeled nuclei (red) in the dorsal, intermediate, and ventral regions. White arrowheads mark multiple PRVeGFP-labeled neurons that colocalize with Chx10. Dotted white lines denote the spinal grey matter. **C**, Enlargement of the boxed area in **B**, shows a PRVeGFP-labeled interneuron that colocalized with Chx10 in lumbar ventral lamina VII. **D**, Two PRVeGFP interneurons were retrogradedly labeled above the complete transection site (~T3-6), and one of them expresses Chx10. Scale bars: **B** = 200 μm, **C**, **D** = 50 μm.

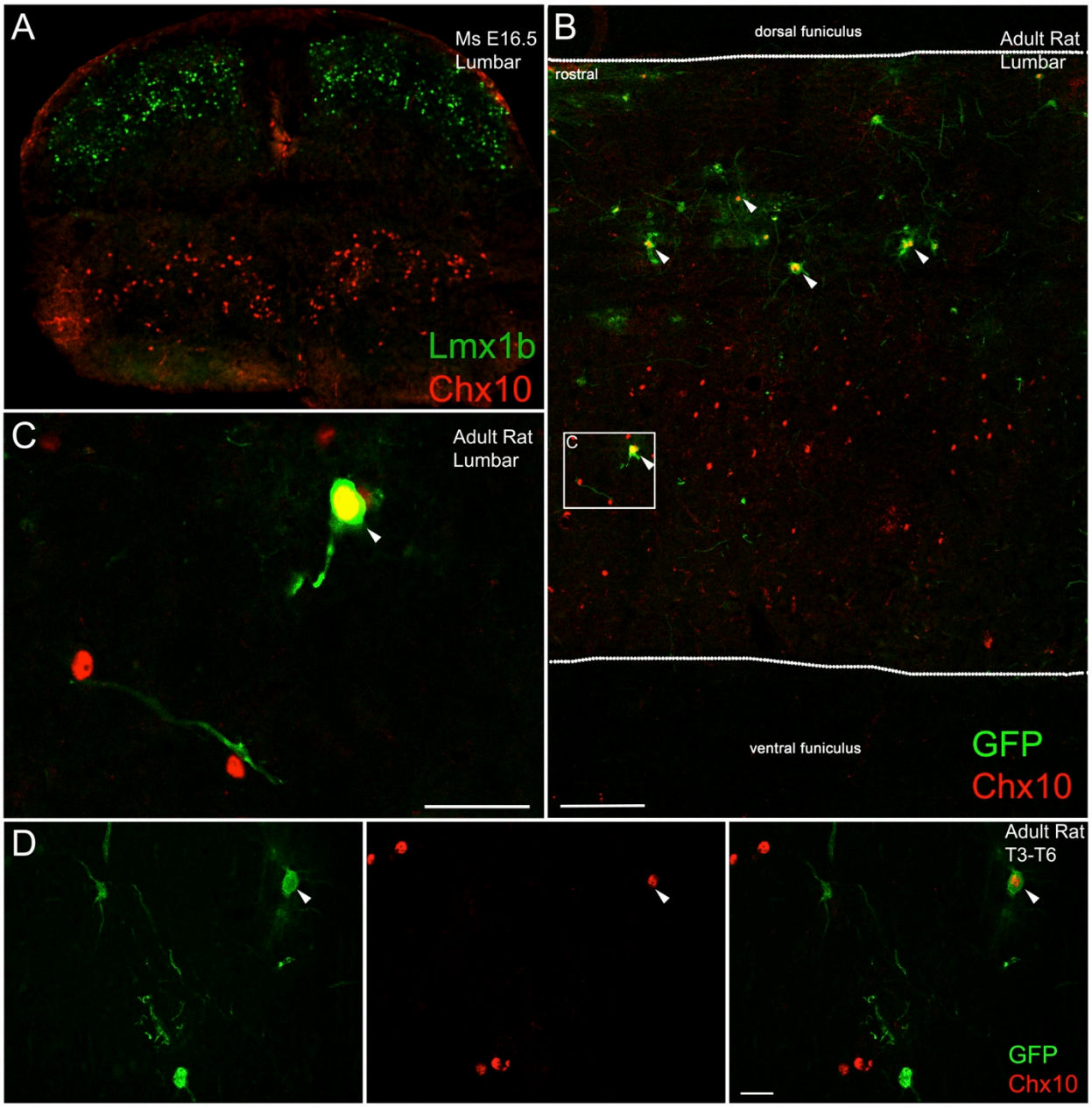
A
Ms E16.5
Lumbar
Lmx1b
Chx10
B
dorsal funiculus
Adult Rat
Lumbar
rostral
C
ventral funiculus
GFP
Chx10
C
Adult Rat
Lumbar
D
Adult Rat
T3-T6
GFP
Chx10

Figure 7.

Lesion volume is larger in FB than OEC-transplanted rats 7 months post transection. **A-B**, To measure lesion volume the sections were processed with GFAP/Aq4 (cyan) to label the reactive astrocytes in the rostral and caudal spinal stumps, and fibronectin (FN, red) to mark the extracellular matrix of the lesion core. The complete transection site is shown in a FB (**A**) and OEC (**B**) -transplanted rat. The OEC-treated rat (**B**) has a near-continuous bridge of GFAP/Aq4 across the injury site and lacks a well-defined lesion core. **C**, Inset from **A**, shows the lesion site contour analysis. A 4000-μm grid was centered on the FN-positive lesion core, and the total cord (white dotted line), lesion core (red), and cysts (yellow) were traced with Neurolucida. The "spared tissue" measure was calculated as the total cord area, with the lesion core and cysts within the spinal stumps subtracted. Lesion volume measures were calculated and normalized to the total volume of the spinal cord. Spared tissue area was normalized to the area of the total cord. **D**, The mean lesion volume ratio was larger in FB than OEC-transplanted rats (p=.046), even with the large variance observed in the OEC group. **E,** The spared tissue ratio did not differ between groups. Boxplots show the group median, interquartile range, and upper and lower whiskers. n = 5 rats/cell transplant group for all comparisons. Scale bars **A, B** = 2000 μm.

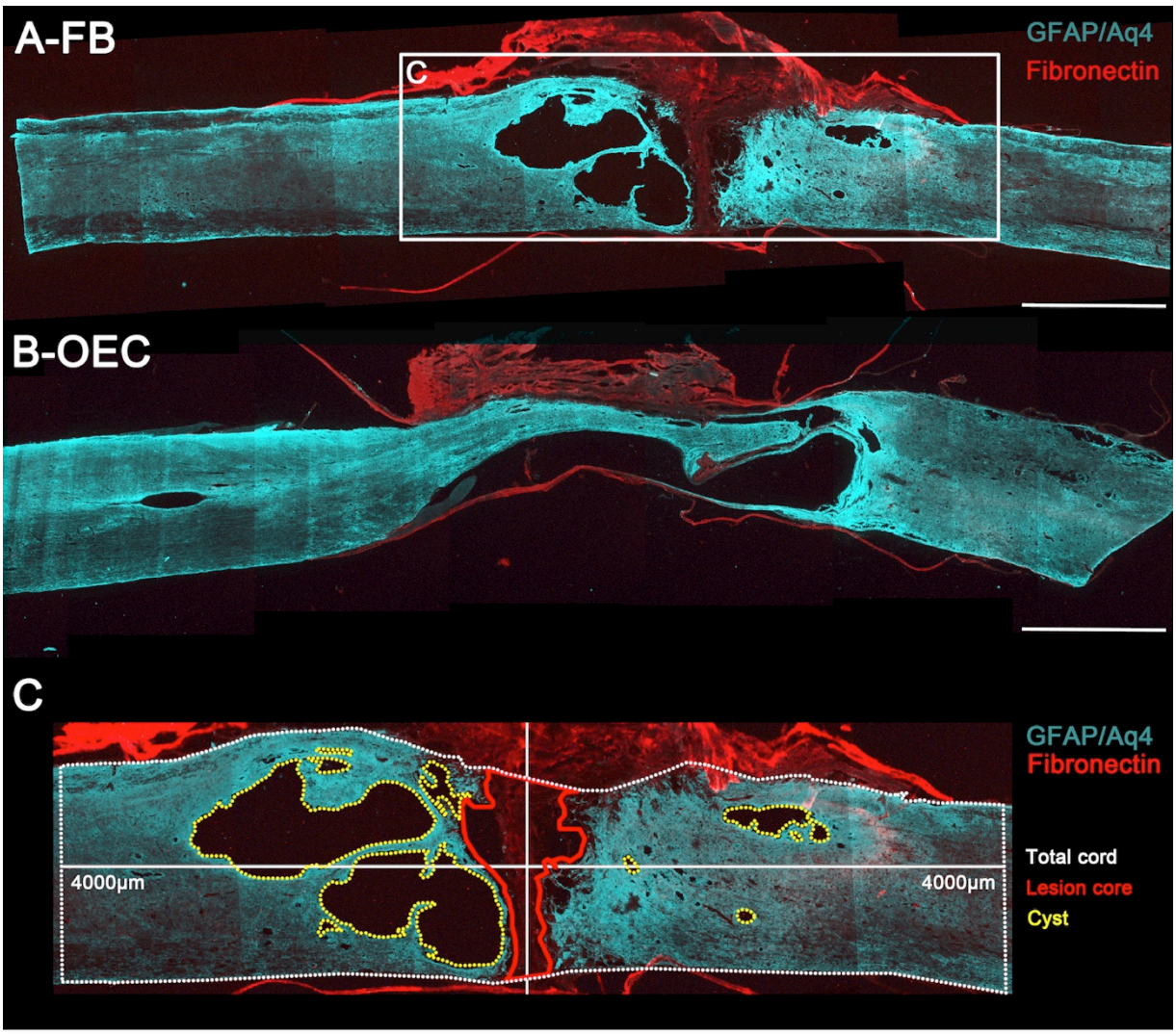
A-FB
C
GFAP/Aq4
Fibronectin
B-OEC
C
GFAP/Aq4
Fibronectin
4000µm
4000µm
Total cord
Lesion core
Cyst

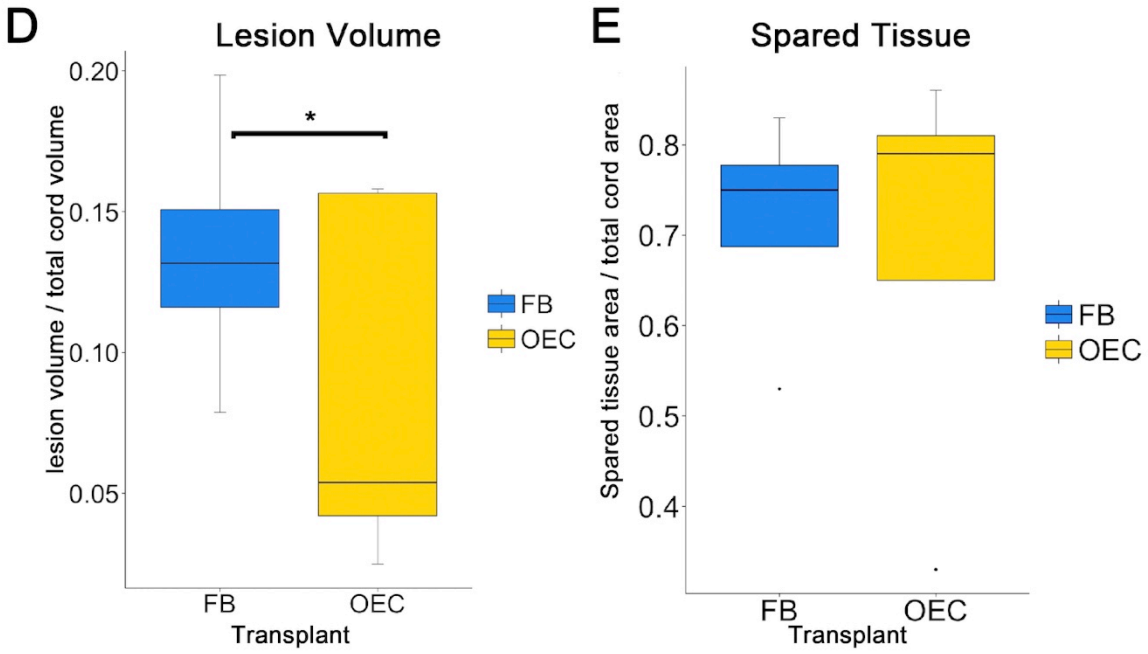
D
Lesion Volume
lesion volume / total cord volume
0.20
0.15
0.10
0.05
*
FB
OEC
FB
OEC
Transplant
E
Spared Tissue
Spared tissue area / total cord area
0.8
0.7
0.6
0.5
0.4
FB
OEC
FB
OEC
Transplant

Figure 8.

Anatomical evidence of axon regeneration in an OEC-transplanted rat. **A**, Six sagittal sections (~400 μm interval) are shown from the OEC-transplanted rat that had PRVeGFP-labeled cells above the injury site. Narrow astrocytic bridges are marked by GFAP labeling (cyan), and appear to cross the complete transection. **B**, Confocal image of **A**-section 3, shows a GFAP-bridge associated with bundles of 5-HT axons that appear to cross the injury site. **C**, An enlargement from **B** shows 5-HT axons that have reached the caudal scar border (white arrowheads) and are within 100 μm of PRVeGFP-labeled cells in the caudal stump (white arrow). **D**, A lateral section shows a clear complete lesion (white dotted line) through this spinal cord. **E-G**, 22 sagittal sections (100 μm) interval were used to reconstruct the spinal cord in three dimensions. **E**, The GFAP-labeled spinal tissue is colored purple, the 5-HT-positive axons are yellow, and PRVeGFP-labeled cells are marked by green dots. The injury site was approximated based on increased translucence of the GFAP reconstruction (**E**, **F**, yellow arrowheads, white dotted lines). When the GFAP and 5-HT traces are removed (**E,** lower image), PRVeGFP-labeled cells are plotted below the injury site (714 cells), within the injury site (44 cells), and above the injury site in the rostral stump (65 cells). **F**, The architecture of the completely transected spinal cord (purple, left) is shown without and with the 5-HT descending axon tracts (yellow, right). **G**, The reconstructed injury site shows 5-HT axon tracts projecting into the caudal spinal stump (white arrowheads) at low (left) and high (right) magnification. Directional arrows on 3D images denote the x (red), y (green), and z-directions (blue). Scale bars: **A** = 1000 μm, **B, C** = 100 μm.

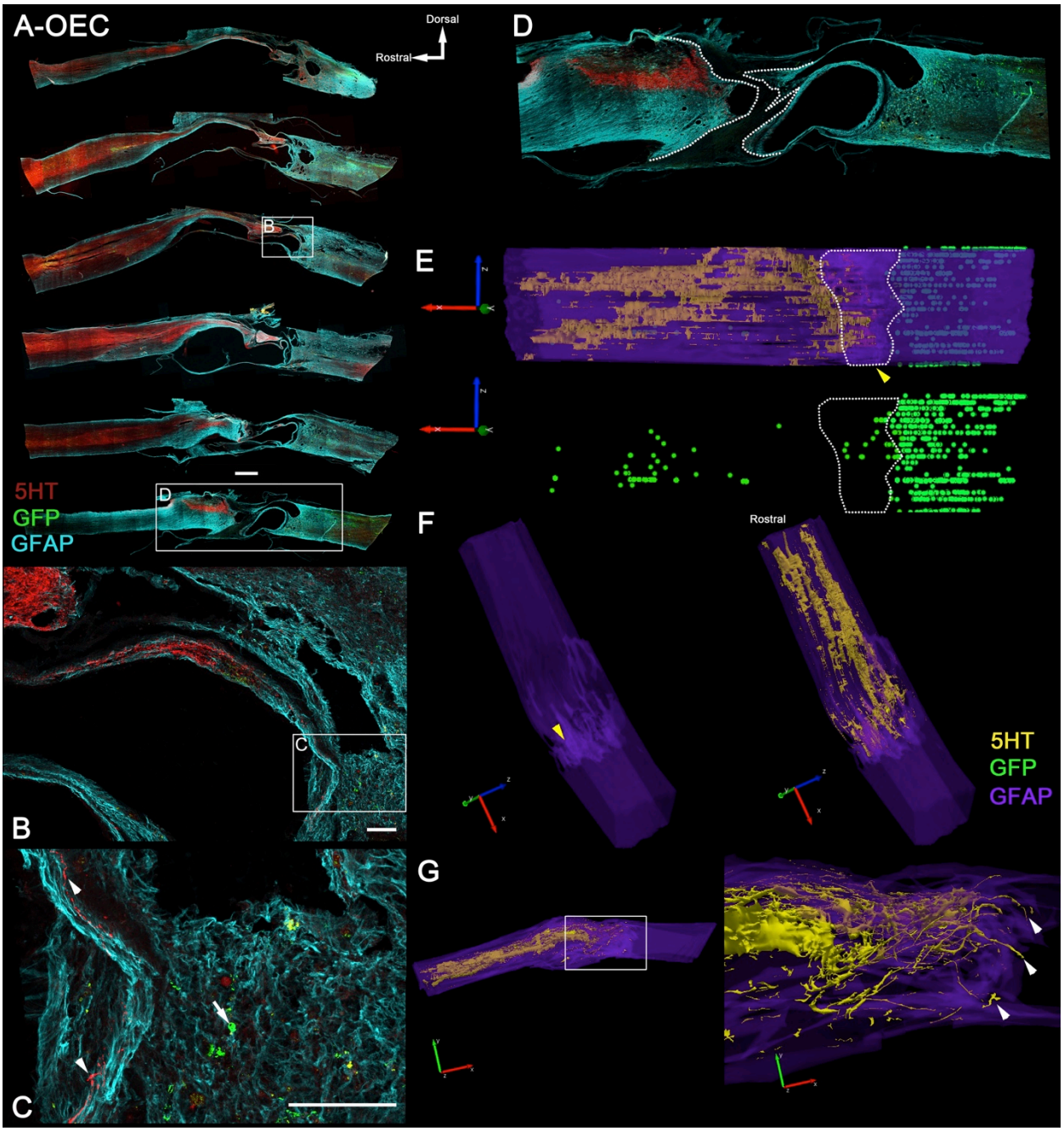
A-OEC
Dorsal
Rostral
B
5HT
GFP
GFAP
D
C
B
C
D
E
F
Rostral
5HT
GFP
GFAP
G

Figure 9.

Evaluation of 5-HT axon bundles that cross the rostral scar border and enter the injury site with astrocyte bridges. **A**, Rostral stump from an OEC-treated rat was immunolabeled with 5-HT (red) and GFAP (cyan). We counted all points where bundles of 5-HT-positive axons crossed the rostral scar border and extended into the lesion core (white arrowheads). **B**, The injury site of an OEC-treated rat has the rostral and caudal stumps, astrocytic extensions, and 5-HT axons highlighted by white, pink, and yellow dotted lines, respectively (top image). Astrocyte extensions were marked at the point their width was less than 100 μm (pink arrowheads). When the rostral and caudal scar borders were traced, the astrocyte extensions were not included (white dotted lines). The bottom image shows only the 5-HT labeling with respect to the glial scar borders. **C**, The mean number of 5-HT axon bundles crossing the rostral scar border was greater in OEC than FB- transplanted rats (p=.04). **D**, The mean area occupied by 5-HT axons within the injury site did not significantly differ in FB vs. OEC-transplanted rats (p=.14). **E**, The mean number of astrocytic extensions tended to be greater on the rostral side in both FB and OEC-transplanted rats (p=.08, p=.19), and there were more astrocyte extensions from the caudal stump of OEC compared to FB-transplanted rats (p=.10). **F**, No statistical difference was observed between FB and OEC-transplanted rats for the GFAP-positive area within the injury site. Scale bars: **A** = 250 μm, **B** = 500 μm.

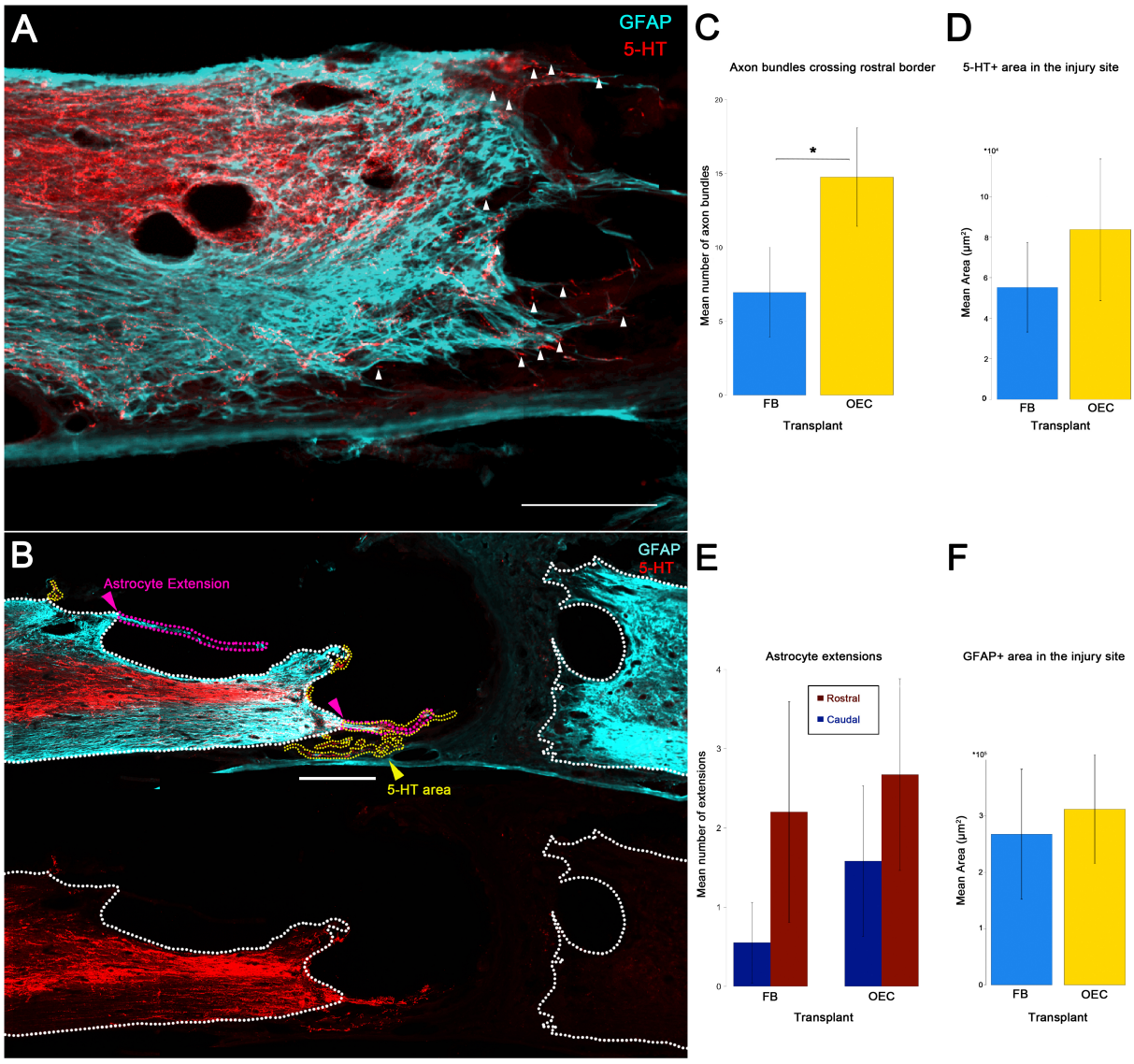
A
GFAP
5-HT
B
GFAP
5-HT
Astrocyte Extension
5-HT area
C
Axon bundles crossing rostral border
Mean number of axon bundles
FB
OEC
Transplant
D
5-HT+ area in the injury site
Mean Area (µm²)
FB
OEC
Transplant
E
Astrocyte extensions
Rostral
Caudal
Mean number of extensions
FB
OEC
Transplant
F
GFAP+ area in the injury site
Mean Area (µm²)
FB
OEC
Transplant

Figure 10.

Bridges of astrocytes are correlated with 5-HT axon regeneration after a complete spinal cord transection. **A-B**, Low-magnification image of the injury site (top) from a FB-transplanted rat that had 5-HT axons crossing the transection. The boxed area is enlarged in a confocal micrograph (bottom) that shows a bridge of 5-HT axons and a PRVeGFP-labeled axon crossing the injury site. High GFAP-immunoreactivity in the rostral stump (yellow arrowhead) made it difficult to visualize astrocytes within the axon bridge. After enlargement, (**B**), it is apparent there are several astrocytes (cyan, white arrowheads) closely associated with the axons that bridge the injury site. **C**, The relationship between astrocyte bridges (GFAP area) and 5-HT axon regeneration (5-HT area) in the injury site was plotted (n = 10 rats). A strong correlation was observed between these two measures (r=.83, *p*=.003). The points that represent the three rats with PRVeGFP-labeling above the injury site are boxed in red. **D**, Low magnification image of the injury site from the second FB-transplanted rat that had PRVeGFP-labeled cells above the injury site. No evidence of axonal regeneration was detected in the injury site. **E**, Low-magnification image of the injury site from the OEC-transplanted rat with PRVeGFP-labeling above the complete transection site. Scale bars **A**, **D**, **E** = 500 μm.

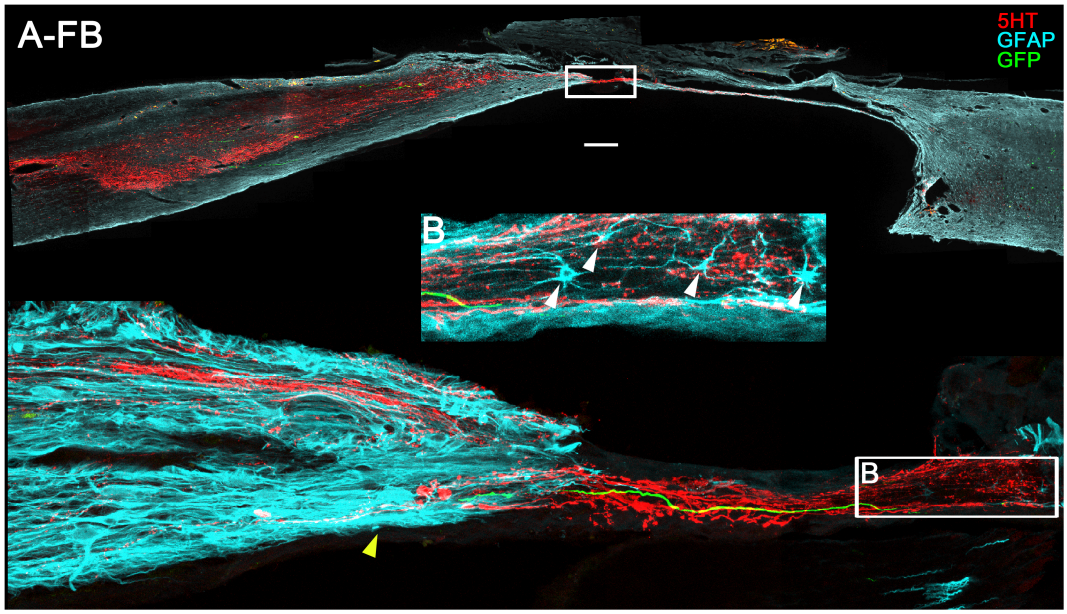
A-FB
5HT
GFAP
GFP
B
B

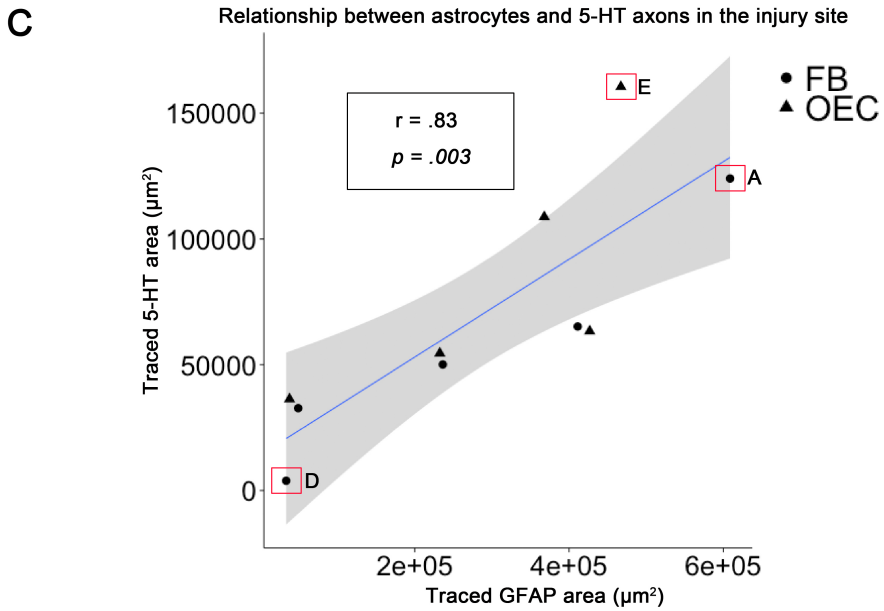
C
Relationship between astrocytes and 5-HT axons in the injury site
r = .83
p = .003
FB
OEC
E
A
D
150000
100000
50000
0
Traced 5-HT area (µm²)
2e+05
4e+05
6e+05
Traced GFAP area (µm²)

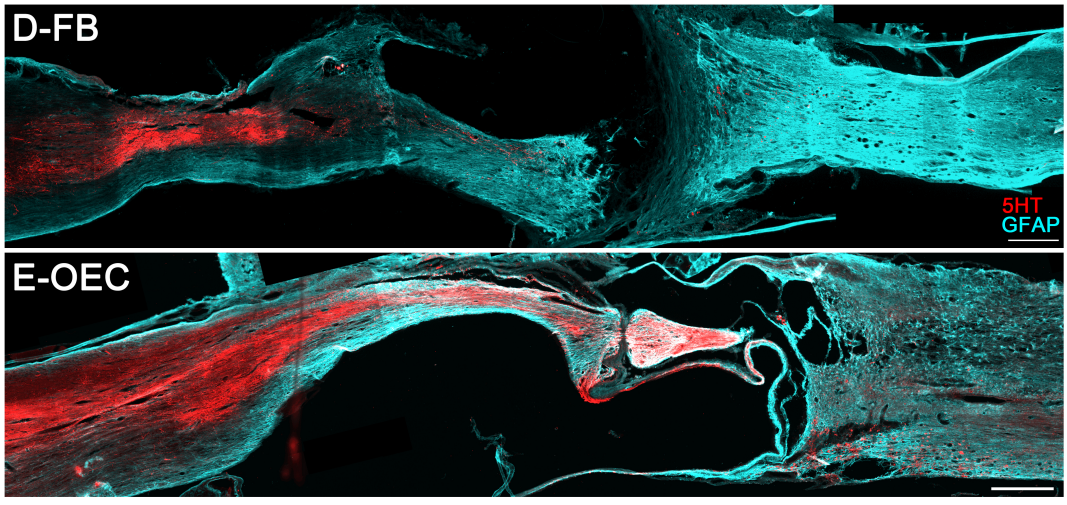
D-FB
5HT
GFAP
E-OEC

References

Alvarez, FJ, Jonas, PC, Sapir, T, Hartley, R, Berrocal, MC, Geiman, EJ, Todd AJ, and Goulding, M (2005) Postnatal phenotype and localization of spinal cord V1 derived interneurons. J Comp Neurol 493(2): 177–192.

Anderson, MA, Burda, JE, Ren, Y, Ao, Y, O'Shea, TM, Kawaguchi, R, Coppola, G, Khakh, BS, Deming, TJ, and Sofroniew, MV (2016) Astrocyte formation aids central nervous system axon regeneration. Nature 532: 195-200.

Arriaga, G, Macopson, JJ, and Jarvis, ED (2015) Transsynaptic tracing from peripheral targets with pseudorabies virus follwed by cholera toxin and biotinylated detran amines double labeling. J Vis Exp 103: e50672.

Arber, S (2012) Motor circuits in action: specification, connectivity, and function. Neuron 74: 975–989.

Bareyre. FM, Kerchensteiner, M, Raineteau, O, Mettenleiter, TC, Weinmann, O, and Schwab, M (2004) The injured rat spinal cord spontaneously forms a new intraspinal circuit in adult rats. Nat Neurosci 7: 269-277.

Borowska, J, Jones, CT, Zhang, H, Blacklaws, J, Goulding, M, and Zhang, Y (2013) Functional subpopulations of V3 interneurons in the mature mouse spinal cord. J Neurosci *33*(47): 18553–65.

Callaway, EM (2008) Transneuronal circuit tracing with neurotropic viruses. Curr Opin Neurobiol 18: 617–23.

Card, JP, Rinaman, L, Lynn, RB, Lee, BH, Meade, RP, Miselis RR, and Enquist, LW (1993) Pseudorabies virus infection of the rat central nervous system: ultrastructural characterization of viral replication, transport, and pathogenesis. J Neurosci 13: 2515–2539.

Card, JP, and Enquist, LW (2014) Transneuronal circuit analysis with pseudorabies viruses. Curr Protoc Neurosci 68: 1.5.1–1.5.39.

Chandler, CE, Parsons, LM, Hosang, M, and Shooter, EM (1984) A monoclonal antibody modulates the interaction of nerve growth factor with PC12 cells. J Biol Chem 259: 6882–6889.

Chung, RS, Woodhouse, A, Fung, S, Dickson TC, West, AK, Vickers, JC, and Chuah, MI (2004) Olfactory ensheathing cells promote neurite sprouting of injured axons in vitro by direct cellular contact and secretion of soluble factors. Cell Mol Life Sci 61:1238–45.

Cornide-Petronio, ME, Ruiz, MS, Barreiro-Iglesias, A, and Rodicio, MC (2011) Spontaneous regeneration of the serotonergic descending innervation in the sea lamprey after spinal cord injury. J Neurotraum *28*(12) 2535–2540.

Courtine, G, Song, B, Roy, RR, Zhong, H, Herrmann, JE, Ao, Y, Qui, J, Edgerton VR, and Sofroniew, MV (2008) Recovery of supraspinal control of stepping via indirect propriospinal relay connections after spinal cord injury. Nat Med 14(1): 69–74.

Cowley, KC, Zaporozhets, E, and Schmidt, BJ (2008) Propriospinal neurons are sufficient for bulbospinal transmission of the locomotor command signal in the neonatal rat spinal cord. J Physiol 586: 1623-35.

Crone, SA, Quinlan, KA, Zagaraiou, L, Droho, S, Restrepo, CE, Lundfald, L, Endo, T, Setlak, J, Jessell, TM, Kiehn, O, and Sharma, K (2008) Genetic ablation of V2a ipsilateral interneurons disrupts left-right locomotor coordination in mammalian spinal cord. Neuron 60: 70-83.

Crone, SA, Zhong, G, Harris-Warrick, R, and Sharma, K (2009) In mice lacking V2a interneurons, gait depends on speed of locomotion. J Neurosci 29: 7098-109.

Dougherty, KJ, and Kiehn, O (2010) Functional organization of V2a-related locomotor circuits in the rodent spinal cord. Ann NY Acad Sci 1198: 85–93.

Edgerton, VR, Leon, RD, Harkema, SJ, Hodgson, JA, London, N, Reinkensmeyer, DJ, Roy, RR, Talmadge, RJ, Tillakaratne, NJ, Timoszyk, W, and Tobin, A (2001) Retraining the injured spinal cord. J Physiol 533: 15–22.

Edgerton, VR, Roy, RR, Hodgson, JA, Prober, RJ, De Guzman, CP, and De Leon, R (1992) Potential of adult mammalian lumbosacral spinal cord to execute and acquire improved locomotion in the absence of supraspinal input. J Neurotraum: 9: 119–28.

Edgerton, VR, Tillakaratne, NJ, Bigbee, AJ, De Leon, RD, and Roy, RR (2004) Plasticity of the spinal neural circuitry after injury. Annu Rev Neurosci 27: 145–167.

Efron, B, and Tibshirani, R (1991) Statistical data analysis in the computer age. Science 253: 390–5.

Enquist, LW (2002) Exploiting circuit-specific spread of pseudorabies virus in the central nervous system: insights to pathogenesis and circuit tracers. J Infect Dis: 186: 209–214.

Filbin, MT (2003) Myelin-associated inhibitors of axonal regeneration in the adult mammalian CNS. Nat Rev Neurosci 4: 703–13.

Filli, L, Engmann, AK, Zörner, B, Weinmann, O, Moraitis, T, Gullo, M, Kasper, H, Schneider, R and Schwab, ME (2014) Bridging the gap: a reticulo-propriospinal detour bypassing an incomplete spinal cord injury. J Neurosci 34: 13399–410.

Filli, L, and Schwab, ME (2015) Structural and functional reorganization of propriospinal connections promotes functional recovery after spinal cord injury. Neural Regen Res 10:

509-513.

Fitch, MT, and Silver, J (2008) CNS injury, glial scars, and inflammation: Inhibitory extracellular matrices and regeneration failure. Exp Neurol 209: 294-301.

Gerasimenko, YP, Avelev, VD, Nikitin, OA, and Lavrov, IA (2003) Initiation of locomotor activity in spinal cats by epidural stimulation of the spinal cord. Neurosci Behav Physiol 33(3): 247–254.

Gerasimenko, YP, Ichiyama, RM, Lavrov, IA, Courtine, G, Cai, L, Zhong, H, Roy, RR, and Edgerton, VR (2007) Epidural spinal cord stimulation plus quipazine administration enable stepping in complete spinal adult rats. J Neurophysiol 98(5): 2525–2536.

Ghosh, M, and Pearse, DD (2014) The role of the serotonergic system in locomotor recovery after spinal cord injury. Front Neural Circuit 8: 151.

Goulding, M (2009) Circuits controlling vertebrate locomotion: moving in a new direction. Nat Rev Neurosci 10(7): 507–518.

Gad, P, Choe, J, Nandra, MS, Zhong, H, Roland RR, Tai, Y, Edgerton, VR (2013) Development of a multi-electrode array for spinal cord epidural stimulation to facilitate stepping and standing after a complete spinal cord injury in adult rats. Neuroeng Rehabil 10: 2.

Gusel'nikova, VV, and Korzhevskiy, DE (2015). NeuN as a neuronal nuclear antigen and neuron differentiation marker. Acta Naturae 7: 42–47.

Iwahara, T, Atsuta, Y, Garcia-Rill, E, and Skinner, RD (1992) Spinal cord stimulation-induced locomotion in the adult cat. Brain Res Bull 28: 99–105.

Harkema, S, Gerasimenko, Y, Hodes, J, Burdick, J, Angeli, C, Chen, Y, Ferreira, C, Willhite, A, Rejc, E, Grossman, RG, and Edgerton, VR (2011) Effect of epidural stimulation of the lumbosacral spinal cord on voluntary movement, standing, and assisted stepping after motor complete paraplegia: A case study. Lancet 377: 1938–1947.

Higginson, JR, and Barnett, SC (2011) The culuture of olfactory ensheathing cells (OECs)–a distinct glial cell type. Exp Neurol 229: 2-9.

Husch, A, Dietz, SB, Hong, DN, and Harris-Warrick, RM (2015) Adult spinal V2a interneurons show increased excitability and serotonin-dependent bistability. J Neurophysiol 113: 1124-34.

Ichiyama, Rm, Gerasimenko, YP, Zhong, H, Roy, RR, and Edgerton VR (2005) Hindlimb stepping movements in complete spinal rats induced by epidural spinal cord stimulation. Neurosci Lett 5: 339-44.

Iyer, S, Maybhate, A, Presacco and All, AH (2010) Multi-limb acquisition of motor evoked

potentials and its application in spinal cord injury. J Neurosci Methods 193: 210-6.

Jovanovic, K, Pastor, AM, and O'Donovan, MJ (2010) The Use of PRV-Bartha to define premotor inputs to lumbar motoneurons in the neonatal spinal cord of the mouse. PloS one 5(7): e11743.

Kafitz, KW, and Greer, CA (1999) Olfactory ensheathing cells promote neurite extension from embryonic olfactory receptor cells in vitro. Glia 25: 99–110.

Kerman, IA, Enquist, LW, Watson, SJ, and Yates, BJ (2003) Brainstem substrates of sympatho-motor circuitry identified using trans-synaptic tracing with pseudorabies virus recombinants. J Neurosci 23: 4657–4666.

Khankan, RR, Wanner, IB, and Phelps, PE (2015) Olfactory ensheathing cell-neurite alignment enhances neurite outgrowth in scar-like cultures. Exp Neurol 269: 93–101.

Khankan, RR, Griffis, KG, Haggerty-Skeans, JR, Zhong, H, Roy, RR, Edgerton, VR, and Phelps, PE (2016) Olfactory ensheathing cell transplantation after a complete spinal cord transection mediates neuroprotective and immunomodulatory mechanisms to facilitate regeneration. J Neurosci 36: 6269-86.

Kubasak, MD, Jindrich, DL, Zhong, H, Takeoka, A, McFarland KC, Muñoz-Quiles, C, Roy, RR, Edgerton, VR, Ramón-Cueto, A, and Phelps, PE (2008) OEG implantation and step training enhance hindlimb-stepping ability in adult spinal transected rats. Brain 131: 264–276.

Lakatos, A, Barnett, SC, and Franklin, RJM (2003) Olfactory ensheathing cells induce less host astrocyte response and chondroitin sulphate proteoglycan expression than Schwann cells following transplantation into adult CNS white matter. Exp Neurol 184(1): 237–246.

Lavrov, I, Gerasimenko, YP, Ichiyama, RM, Courtine, G, Zhong, H, Roy, RR, and Edgerton, VR (2006) Plasticity of spinal cord reflexes after a complete transection in adult rats: relationship to stepping ability. J Neurophysiol 96(4): 1699–1710.

Lewis, DI, and Coote, JH (1990) The influence of 5-hydroxytryptamine agonists and antagonists on identified sympathetic preganglionic neurones in the rat, in vivo. Br J Pharmacol 99: 667–672

Lee, JK, and Zheng, B (2012) Role of myelin-associated inhibitors in axonal repair after spinal cord injury. Exp Neurol 235: 33-42.

Li, S, Kim, JE, Budel, S, Hampton, TG, and Strittmatter, SM (2005) Transgenic inhibition of Nogo-66 receptor function allows axonal sprouting and improved locomotion after spinal injury. Mol Cell Neurosci 29(1): 26–39.

Li, Y, Li, D, and Raisman, G (2005) Interaction of olfactory ensheathing cells with astrocytes may be the key to repair of tract injuries in the spinal cord: The "pathway hypothesis." J

Neurocytol 34: 343-51.

Li, Y, and Raisman, G (2007) Repair of neural pathways by olfactory ensheathing cells. Nat Rev Neurosci 8: 312-319.

Lichtman, JW, Purves, D, and Yip, JW (1980) Innervation of sympathetic neurones in the guinea-pig thoracic chain. J Physiol 298: 285–299.

Lipson, AC, Widenfalk, J, Lindqvist, E, Ebendal, T, and Olson, L (2003) Neurotrophic properties of olfactory ensheathing glia. Exp Neurol 180(2): 167–171.

Lu, J, Féron, F, Mackay-Sim, A, and Waite, PME (2002) Olfactory ensheathing cells promote locomotor recovert after delayed transplantation into transected spinal cord. Brain 125: 14–21.

Lukovic, D, Manzano, MV, Mocholi, EL, Rodriguez-Jimenez, FJ, Jendelova, P, Sykova, E, Oria, M, Stojkovic, M, and Erceg, S (2015) Complete spinal cord transection as a faithful model of spinal cord injury for translational cell transplantation. Sci Rep 5: 9640.

Lynskey, JV, Belanger, MS, and Jung, R (2008) Activity-dependent plasticity in spinal cord injury. J Rehabil Res Dev 45: 229-40.

McCall, RB (1983) Serotonergic excitation of sympathetic preganglionic neurons: a microiontophoretic study. Brain Res 289: 121-7.

McKeon, RJ, Jurynec, MJ, and Buck, CR (1999) The chondroitin sulfate proteoglycans neurocan and phosphacan are expressed by reactive astrocytes in the chronic CNS glial scar. J Neurosci 19: 10778-88.

Miles, GB, Hartley, R, Todd, AJ, and Brownstone, RM (2006) Spinal cholinergic interneurons regulate the excitability of motoneurons during locomotion. Proc Natl Acad Sci 104: 2448–2453.

Moran-Rivard, L, Kagawa, T, Saueressig, H, Gross, MK, Burrill, J, and Goulding, M (2001) Evx1 is a postmitotic determinant of V0 interneuron identity in the spinal cord. Neuron 29(2): 385–399.

Nazareth, L, Lineburg, KE, Chuah, MI, Tello Velasquez, J, Chehrehasa, F, St John, JA, and Ekberg, JAK (2015) Olfactory ensheathing cells are the main phagocytic cells that remove axon debris during early development of the olfactory system. J Comp Neurol 523(3): 479–494.

Ni, Y, Nawabi, H, Liu, X, Yang, L, Miyamichi, K, Tedeschi, A, Xu, B, Wall, NR, Callaway, EM, and He, Z (2014) Characterization of long descending premotor propriospinal neurons in the spinal cord. J Neurosci 34(28): 9404–17.

Njå, A, and Purves, D (1977) The effects of nerve growth factor and its antiserum on synapses in the superior cervical ganglion of the guinea-pig. J Physiol 277: 53-75.

O'Toole, DA, West, AK, and Chuah, MI (2007) Effect of olfactory ensheathing cells on reactive astrocytes in vitro. Cell Mol Life Sci 64(10): 1303–9.

Perry, AC, Wakayama, T, Kishikawa, H, Kasai, T, Okabe, M, Toyoda, Y, and Yanagimachi, R (1999) Mammalian transgenesis by intracytoplasmic sperm injection. Science 284: 1180–1183.

Pellitteri, R, Spatuzza, M, Russo, A, Zaccheo, D, and Stanzani, S (2009) Olfactory ensheathing cells represent an optimal substrate for hippocampal neurons: an in vitro study. Int J Dev Neurosci 27 453–8.

Phelps, PE, Barber, RP, Houser, CR, Crawford, GD, Salvaterra, PM, and Vaughn, JE (1984) Postnatal development of neurons containing choline acetyltransferase in rat spinal cord: an immunocytochemical study. J Comp Neurol 229: 347-61.

Pickering, AE, Spanswick, D, and Logan, SD. (1994) 5-Hydoxytryptamine evokes depolarizations and membrane potential oscillations in rat sympathetic preganglionic neurones. J Physiol 480: 109–121

Pierani, A, Moran-Rivard, L, Sunshine, MJ, Littman, DR, Goulding, M, and Jessell, TM (2001) Control of interneuron fate in the developing spinal cord by the progenitor homeodomain protein Dbx1. Neuron 29(2): 367–384.

Ramón-Cueto, A, Cordero, MI, Santos-Benito, FF, and Avila, J (2000) Functional recovery of paraplegic rats and motor axon regeneration in their spinal cords by olfactory ensheathing glia. Neuron 25(2): 425–435.

Rejc, E, Angeli, C, and Harkema, S (2015) Effects of lumbosacral spinal cord epidural stimulation for standing after chronic complete paralysis in humans. PLoS ONE 10(7).

Rotto-Percelay, DM, Wheeler, JG, Osorio, FA, Platt, KB, and Loewy, AD (1992) Transneuronal laeling of spinal interneurons and sympathetic preganglionic neurons after pseduorabies virus injections in the rat medial gastrocnemius muscle. Brain Res 574: 291–306.

Roy, RR, Hodgson, JA, Lauretz, SD, Pierotti, DJ, Gayek, RJ, and Edgerton, VR (1992) Chronic spinal cord-injured cats: Surgical procedures and management. Lab Anim Sci 42: 335-343.

Runyan, SA, and Phelps, PE (2009) Mouse olfactory ensheathing glia enhance axon outgrowth on a myelin substrate in vitro. Exp Neurol 216(1): 95–104.

Sofroniew, MV (2009). Molecular dissection of reactive astrogliosis and glial scar formation. Trend Neurosci 32: 638-47.

Stepien, AE, Tripodi, M, and Arber, S (2010) Monosynaptic rabies virus reveals premotor network organization and synaptic specificity of cholinergic partirition cells. Neuron 68: 456-72.

Tabakow, P, Raisman, G, Fortuna, W, Czyz, M, Huber, J, Li, D, Szewczyk, P, Okurowski, S, Miedzybrodzki, R, Czapiga, B, Salomon, B, Halon, S, Li, Y, Lipiec, J, Kulczyk, A and Jarmundowicz, W (2014) Functional regeneration of supraspinal connections in a patient with transected spinal cord following transplantation of bulbar olfactory ensheathing cells with peripheral nerve bridging. Cell Transplant 23: 1631-55.

Takeoka, A, Jindrich, DL, Muñoz-Quiles, C, Zhong, H, van den Brand, R, Pham, DL, Ziegler, MD, Ramón-Cueto, A, Roy, RR, Edgerton, VR, and Phelps, PE (2011) Axon regeneration can facilitate or suppress hindlimb function after olfactory ensheathing glia transplantation. J Neurosci 31: 4298–4310.

Takeoka, A, Kubasak, MD, Zhong, H, Roy, RR, and Phelps, PE (2009) Serotonergic innervation of the caudal spinal stump in rats after complete spinal transection: Effect of olfactory ensheathing glia. Journal Comp Neurol 515(6): 664–676.

Thaler, J, Harrison, K, Sharma, K, Lettieri, K, Kehrl, J, and Pfaff, SL (1999) Active suppression of interneuron programs within developing motor neurons revealed by analysis of homeodomain factor HB9. Neuron 23: 675-87.

Thaler, JP, Lee, SK, Jurata, JW, Gill, GN, and Pfaff, SL (2002) LIM factor Lhx3 contributes to the specification of motor neuron and interneuron identity through cell-type-specific protein-protein interactions. Cell 110(2): 237–249.

Tillakratne, NJ, Guu, JJ, de Leon, RD, Bigbee, AJ, London, NJ, Zhong, H, Ziegler, MD, Joynes, RL, Roy, RR, and Edgerton, VR (2010) Functional recovery of stepping in rats after a complete neonatal spinal cord transection is not due to regrowth across the lesion site. Neuroscience 166: 23-33.

Vallstedt, A, Muhr, J, Pattyn, A, Pierani, A, Mendelsohn, M, Sander, M, Jessell TM, and Ericson, J (2001) Different levels of repressor activity assign redundant and specific roles to Nkx6 genes in motor neuron and interneuron specification. Neuron 31(5): 743–755.

Vavrek, R, Girgis, W, Tetzlaff, G, Hiebert, W, and Fouad, K (2006) BDNF promotes connections of corticospinal neurons onto spared descending interneurons in spinal cord injured rats. Brain 129: 1534-1545.

von Euler, M, Janson, AM, Larsen, JO, Seiger, A, Forno, L, Bunge, MB, and Sundström, E (2002) Spontaneous axonal regeneration in rodent spinal cord after ischemic injury. J Neuropathol Exp Neurol 61: 64–75.

Wallis, DI, and North, RA (1978) The action of 5-hydroxytryptamine on single neurones of the rabbit superior cervical ganglion. Neuropharmacology 17: 1023-1028.

Wanner, IB, Anderson, MA, Song, B, Levine, J, Fernandez, A, Gray-Thompson, Z, Ao, Y, and Sofroniew, MV (2013) Glial scar borders are formed by newly proliferated, elongated astrocytes that interact to corral inflammatory and fibrotic cells via STAT3-dependent mechanisms after spinal cord injury. J Neurosci 33(31): 12870–86.

Watts, SW, Morrison, SF, Davis, RP, and Barman, SM (2012) Serotonin and blood pressure regulation. Pharmacol Rev 64: 359-388.

Witts, EC, Zagoraiou, L, and Miles, GB (2014) Anatomy and function of cholinergic C bouton inputs to motor neurons. J Anat 224: 52-60.

Wolpaw, JR, and Tennissen, AM (2001) Activity-dependent spinal cord plasticity in health and disease. Ann Rev Neurosci 24: 807–43.

Woodhall, E, West, AK, and Chuah, MI (2001) Cultured olfactory ensheathing cells express nerve growth factor, brain-derived neurotrophic factor, glia cell line-derived neurotrophic factor and their receptors. Brain Res 88(1-2): 203–213.

Yang, M, Card, JP, Tirabassi, RS, Miselis RR, and Enquist LW (1999) Retrograde, transneuronal spread of pseudorabies virus in defined neuronal circuitry of the rat brain is facilitated by gE mutations that reduce virulence. J Virol 73: 4350–4359.

Zagoraiou, L, Akay, T, Martin, JF, Brownstone, RM, Jessell, TM, and Miles, GB (2009) A cluster of cholinergic premotor interneurons modulates mouse locomotor activity. Neuron 64: 645-62.

Zhang, Y, Narayan, S, Geiman, E, Lanuza, GM, Velasquez, T, Shanks, B, Akay, T, Dyck, J, Pearson, K, Gosgnach, S, Fan, CM, and Goulding, M (2008) V3 spinal neurons establish a robust and balanced locomotor rhythm during walking. Neuron 60: 84-96.

Zhong, G, Droho, S, Crone, SA, Dietz, S, Kwan, AC, Webb, WW, Sharma, K, and Harris-Warrick, RM (2010) Electrophysiological characterization of V2a interneurons and their locomotor-related activity in the neonatal mouse spinal cord. J Neurosci 30(1): 170–182.

Zhou, Y, Yamamoto, M, and Engel, JD (2000) GATA2 is required for the generation of V2 interneurons. Development 127(17): 3829–3838.

Ziegler, MD, Hsu, D, Takeoka, A, Zhong, H, Ramón-Cueto, A, Phelps, PE, Roy, RR, and Edgerton, VR (2011) Further evidence of olfactory ensheathing glia facilitating axonal regeneration after a complete spinal cord transection. Exp Neurol 229: 109– 19.